A Dual Boundary Element based Implicit Differentiation Method for Determining Stress Intensity Factor Sensitivities for Plate Bending Problems

Llewellyn Morse*, Zahra Sharif Khodaei, M.H. Aliabadi

Department of Aeronautics, Imperial College London, South Kensington Campus, City and Guilds Building, Exhibition Road, SW7 2AZ, London, UK

Abstract

A novel methodology for determining Stress Intensity Factor (SIF) sensitivities for plate bending problems using the Dual Boundary Element Method (DBEM) is presented. The direct derivatives of the DBEM integral equations for plate bending have been derived for the first time and are used as part of a DBEM-based Implicit Differentiation Method (IDM or DBEM-IDM) for calculating the sensitivities of SIFs to changes in different geometric parameters such as crack length and crack rotation angle. The SIFs and their sensitivities are calculated using the J-integral and the derivative of the J-integral respectively. A numerical example featuring a thick plate subjected to membrane, bending, and pressure loads is presented. In the first half of the numerical example, the SIF sensitivities from the IDM are compared with those obtained from the more common, but relatively crude, Finite Difference Method (FDM or DBEM-FDM). Results show that the IDM is a significantly more efficient and robust alternative to the FDM. The accuracy of the FDM showed significant dependence on the step size used, necessitating a time-consuming optimization procedure to determine the optimal step size. Once this optimal step size was found, both methods provided very similar results. As part of the second half of the numerical example, a demonstration of one possible application of the SIF sensitivities from the IDM is presented. This involved carrying out reliability analyses using the First-Order Reliability Method (FORM) with a large number of design variables.

Keywords: Dual Boundary Element Method (DBEM); Implicit Differentiation Method (IDM); Finite Difference Method (FDM); Stress Intensity Factor (SIF); Plate Bending

1. Introduction

It is well established that knowledge of the Stress Intensity Factor (SIF) is necessary for the evaluation of the residual strength of flawed components. Over the past fifty years many methods of calculating SIFs have been developed and recorded in the Compendium of Stress Intensity Factors [1]. These SIF solutions include simple numerical methods such as the Green's function [2], Compounding [3], and also more advanced methods such as the Weight Function [4].

As well as the SIFs themselves, their sensitivities with respect to changes in different structural design variables are also particularly important, as they enable engineers to understand how to mitigate crack growth and

*Corresponding author

Email addresses: llewellyn.morse12@imperial.ac.uk (L. Morse), z.sharif-khodaei@imperial.ac.uk (Z. Sharif Khodaei), m.h.aliabadi@imperial.ac.uk (M.H. Aliabadi)

Abbreviations: Dual Boundary Element Method (DBEM); Finite Element Method (FEM); Implicit Differentiation Method (IDM); Finite Difference Method (FDM); First-Order Reliability Method (FORM)

make their designs safer. Since the value of many design variables is often uncertain, the adequate performance of a structure is not guaranteed, therefore a probability that the structure fails to perform adequately needs to be defined, this probability is termed the *probability of failure*. The sensitivity of SIFs is often required to predict the probability of failure for failure modes related to crack growth. These sensitivities can be used with reliability methods such the First-Order Reliability Method (FORM) [5] to evaluate the probability of failure.

The Dual Boundary Element Method (DBEM) is used in this work with the J-integral to evaluate SIF sensitivities with respect to changes in geometric design variables. The DBEM has proven itself to be an efficient alternative to the Finite Element Method (FEM) for applications related to fracture mechanics. In contrast to the FEM, the DBEM only requires the outer boundaries of a structure to be discretised, enabling it to provide a continuous modelling of the interior of the structure, providing high-resolution internal displacements and stresses. Since the J-integral involves the evaluation of displacement and stresses at internal points in the structure, the combined use of the DBEM and the J-integral can provide very accurate estimates for SIFs. Detailed discussions related to other advantages and potential applications of the DBEM can be found in [6].

The DBEM for plate problems involving combined bending and tension was first developed by Dirgantara and Aliabadi [7]. In this approach, Reissner plate theory is used to model plate bending and shear, while 2D plane stress theory is used to model the behaviour of the plate membrane. Reissner theory is used instead of Kirchoff theory since it is able to obtain crack tip stress fields that show better agreement to those provided by 3D elasticity [8]. The approach outlined in [7] has since been adapted to a wide range of problems, the most relevant of which include: the analysis of cracks in structures undergoing large deflection [9], dynamic fracture mechanics [10], fatigue crack growth in assembled plate structures [11], and the analysis of bond-line cracks in laminated plates [12]. Among the different Boundary Element methods used to solve problems involving fracture mechanics with Reissner plates, the DBEM is the most commonly used. However, one other method used in the past involves the use of the Numerical Green's Function (NGF) technique [13]. Building on this previous work concerning the DBEM, the approach outlined in [7] is adapted in this current work for the calculation of the sensitivities of SIFs to changes in various geometric parameters in plate bending problems involving combined bending and tension. Potential applications include reliability analysis and shape optimisation.

One recent variation of the BEM is the isogeometric BEM [14, 15, 16]. The isogeometric BEM involves the use of Non-Uniform Rational B-Splines (NURBS) to represent the boundaries of the structure. Since NURBS are also commonly used in Computer Aided Design (CAD), data can be transferred between isogeometric BEM and CAD tools relatively easily [16]. Some relevant past examples of its use include applications to fracture mechanics, [14, 15] and shape optimisation [16].

Methods used in the past for the calculation of SIF sensitivities have involved the use of the Finite Element Method (FEM) [17, 18], the Fractal Finite Element Method (FFEM) [19], the Scaled Boundary Finite Element Method (SBFEM) [20, 21], the eXtended Finite Element Method (XFEM) [22], Galerkin Meshless Methods [23, 24] , and the Dual Boundary Element Method (DBEM) [25]. SIF sensitivities are usually taken with respect to geometric design variables such as crack length or crack rotation angle. One notable example of previous work concerning SIF sensitivity calculation is Huang and Aliabadi [25] where a DBEM-based Implicit Differentiation Method (IDM), which makes use of the derivatives of the two-dimensional DBEM integral equations, was used to evaluate SIF sensitivities in two-dimensional structures. Results were validated against the FDM with the DBEM and the FEM. Previous work concerning the calculation of SIF sensitivities has exclusively focused on two-dimensional structures. However, aircraft structures such as wing panels and fuselage panels are often

subjected to bending loads and pressure loads. It is therefore more appropriate to model them as thick plates or shells. This is the approach taken in this work.

Two methods are investigated in this work for the calculation of SIF sensitivities using the DBEM - the Finite Difference Method (FDM) and an Implicit Differentiation Method (IDM). The FDM is a relatively crude method involving the use of finite differences to calculate derivatives. The accuracy of the sensitivities from the FDM can be very dependent on the step size used - if the step size is too small or too large then rounding errors or truncation errors, respectively, become significant. An IDM, on the other hand, involves the derivation of the exact derivatives of the DBEM integral equations with respect to some geometric variable. Since an IDM does not require the use of a step size, it is significantly more robust than the FDM, and can provide sensitivities that are much more accurate and reliable. Past examples of the use of BEM-based IDMs includes [25, 26, 27]. One notable example is Sfantos and Aliabadi [26] where a BEM-based IDM was employed for evaluating design sensitivities for contact problems. The results from the IDM were validated against an analytical solution and against a BEM-based FDM. It showed close agreement with both methods. In this current work, the use of the FDM or the IDM with the DBEM is hereafter referred to as DBEM-based FDM (DBEM-FDM) or DBEM-based IDM (DBEM-IDM) respectively.

The main objective of this work was to create a DBEM-based IDM that acts as a much more efficient and robust alternative to the relatively crude DBEM-based FDM when evaluating SIF sensitivities with respect to geometric design variables for plate bending problems. Previous work on this topic has exclusively focused on two-dimensional structures. To achieve this objective, a DBEM-based IDM for plate bending has been developed for the first time. This DBEM-IDM makes use of the derivatives of the DBEM integral equations and the J-integral formulations for plate bending. These derivatives have also been derived for the first time and are presented here. To validate the proposed DBEM-IDM, SIF sensitivities are compared with those from a DBEM-based FDM. To demonstrate one possible application of the DBEM-IDM, it is used in the reliability analysis of a thick plate subjected to membrane, bending, and pressure loads with the FORM.

2. Methodology

In this work, Latin letter indexes (e.g. i, j, k) can take values from 1 to 3, while Greek letter indexes (e.g. α, β, ρ, γ) can takes values of either 1 or 2.

2.1. DBEM for Plate Bending Problems

From [7], the discretised DBEM integral equations for plate bending are:

$$\frac{1}{2}w_j(\mathrm{x}^+) + \frac{1}{2}w_j(\mathrm{x}^-) + \sum_{n_e=1}^{N_e}\sum_{\gamma=1}^{M} P_{ij}^{b,n_e\gamma} w_j^{n_e\gamma} = \sum_{n_e=1}^{N_e}\sum_{\gamma=1}^{M} Q_{ij}^{b,n_e\gamma} p_j^{n_e\gamma} + q_3 \sum_{n_e=1}^{N_e} O_i^{b,n_e} \tag{1}$$

where:

$$P_{ij}^{b,n_e\gamma} = \int_{-1}^{+1} T_{ij}^b(\mathrm{x}^+, \mathrm{x}(\eta)) N^{n_e\gamma}(\eta) J^{n_e}(\eta) d\eta \tag{2}$$

$$Q_{ij}^{b,n_e\gamma} = \int_{-1}^{+1} U_{ij}^b(\mathrm{x}^+, \mathrm{x}(\eta)) N^{n_e\gamma}(\eta) J^{n_e}(\eta) d\eta \tag{3}$$

$$O_i^{b,n_e} = \int_{-1}^{+1} B_i^b(\mathrm{x}^+, \mathrm{x}(\eta)) J^{n_e}(\eta) d\eta \tag{4}$$

and:

$$B_i^b(\mathrm{x}^+, \mathrm{x}(\eta)) = V_{i,\alpha}^b(\mathrm{x}^+, \mathrm{x}) n_\alpha(\mathrm{x}) - \frac{\nu}{(1-\nu)\lambda^2} U_{i\alpha}^b(\mathrm{x}^+, \mathrm{x}) n_\alpha(\mathrm{x}(\eta)) \tag{5}$$

for the displacement integral equation, and:

$$\frac{1}{2}p_i(\mathrm{x}^-) - \frac{1}{2}p_i(\mathrm{x}^+) + n_\beta(\mathrm{x}^-)\sum_{n_e=1}^{N_e}\sum_{\gamma=1}^{M} K_{i\beta k}^{b,n_e\gamma} w_k^{n_e\gamma} = n_\beta(\mathrm{x}^-)\sum_{n_e=1}^{N_e}\sum_{\gamma=1}^{M} L_{i\beta k}^{b,n_e\gamma} p_k^{n_e\gamma} + n_\beta(\mathrm{x}^-) q_3 \left(\sum_{n_e=1}^{N_e} O_{i\beta}^{*,n_e} + \delta_{i\beta}\frac{\nu}{(1-\nu)\lambda^2} \right) \tag{6}$$

where:

$$K_{i\beta k}^{b,n_e\gamma} = \oint_{-1}^{+1} S_{i\beta k}^{b}(\mathrm{x}^-, \mathrm{x}(\eta)) N^{n_e\gamma}(\eta) J^{n_e}(\eta) d\eta \tag{7}$$

$$L_{i\beta k}^{b,n_e\gamma} = \oint_{-1}^{+1} D_{i\beta k}^{b}(\mathrm{x}^-, \mathrm{x}(\eta)) N^{n_e\gamma}(\eta) J^{n_e}(\eta) d\eta \tag{8}$$

$$O_{i\beta}^{*,n_e} = \oint_{-1}^{+1} B_{i\beta}^{*}(\mathrm{x}^-, \mathrm{x}(\eta)) J^{n_e}(\eta) d\eta \tag{9}$$

and:

$$B_{i\beta}^{*}(\mathrm{x}^-, \mathrm{x}(\eta)) = Q_{i\beta}^{*}(\mathrm{x}^-, \mathrm{x}(\eta)) - \frac{\nu}{(1-\nu)\lambda^2} D_{i\beta\rho}^{b}(\mathrm{x}^-, \mathrm{x}(\eta)) n_\rho(\mathrm{x}(\eta)) \tag{10}$$

for the traction integral equation.

The DBEM integral equations for two-dimensional plane stress (membrane) are:

$$\frac{1}{2}u_\beta(\mathrm{x}^+) + \frac{1}{2}u_\beta(\mathrm{x}^-) + \sum_{n_e=1}^{N_e}\sum_{\gamma=1}^{M} P_{\alpha\beta}^{n_e\gamma} u_\beta^{n_e\gamma} = \sum_{n_e=1}^{N_e}\sum_{\gamma=1}^{M} Q_{\alpha\beta}^{n_e\gamma} t_\beta^{n_e\gamma} \tag{11}$$

where:

$$P_{\alpha\beta}^{n_e\gamma} = \oint_{-1}^{+1} T_{\alpha\beta}(\mathrm{x}^+, \mathrm{x}(\eta)) N^{n_e\gamma}(\eta) J^{n_e}(\eta) d\eta \tag{12}$$

$$Q_{\alpha\beta}^{n_e\gamma} = \int_{-1}^{+1} U_{\alpha\beta}(\mathrm{x}^+, \mathrm{x}(\eta)) N^{n_e\gamma}(\eta) J^{n_e}(\eta) d\eta \tag{13}$$

for the displacement integral equation, and:

$$\frac{1}{2}t_\alpha(\mathrm{x}^-) - \frac{1}{2}t_\alpha(\mathrm{x}^+) + n_\beta(\mathrm{x}^-)\sum_{n_e=1}^{N_e}\sum_{\gamma=1}^{M} K_{\rho\alpha\beta}^{n_e\gamma} u_\rho^{n_e\gamma} = n_\beta(\mathrm{x}^-)\sum_{n_e=1}^{N_e}\sum_{\gamma=1}^{M} L_{\rho\alpha\beta}^{n_e\gamma} t_\rho^{n_e\gamma} \tag{14}$$

where:

$$K_{\rho\alpha\beta}^{n_e\gamma} = \oint_{-1}^{+1} S_{\rho\alpha\beta}(\mathrm{x}^-, \mathrm{x}(\eta)) N^{n_e\gamma}(\eta) J^{n_e}(\eta) d\eta \tag{15}$$

$$L_{\rho\alpha\beta}^{n_e\gamma} = \oint_{-1}^{+1} D_{\rho\alpha\beta}(\mathrm{x}^-, \mathrm{x}(\eta)) N^{n_e\gamma}(\eta) J^{n_e}(\eta) d\eta \tag{16}$$

for the traction integral equation.

In the above equations, T_{ij}^b, U_{ij}^b, $V_{i,\alpha}^b$, $S_{i\beta k}^b$, $D_{i\beta k}^b$, and $Q_{i\beta}^*$ are the fundamental solutions for plate bending, while $T_{\alpha\beta}$, $U_{\alpha\beta}$, $S_{\alpha\beta\rho}$, and $D_{\alpha\beta\rho}$ are the fundamental solutions for the membrane. Expressions for these fundamental solutions can be found in [6]. The integral symbols $\oint$ and $\oint\!\!\!\!=$ represent Cauchy principal value integrals and Hadamard principal value integrals respectively. w_1 and w_2 denote rotations in the directions x_1 and x_2 respectively, and w_3 denotes displacement in the direction x_3. u_1 and u_2 are the displacements in the directions x_1 and x_2 respectively. p_k are the bending and shear tractions with $p_\alpha = M_{\alpha\beta}n_\beta$ and $p_3 = Q_\alpha n_\alpha$. t_1 and t_2 are membrane tractions in the directions x_1 and x_2 respectively where $t_\alpha = N_{\alpha\beta}n_\beta$. The integrations are carried out over the boundary S of the structure's domain. n_β denotes the components of the unit outward normal vector at the boundary. x^+ and x^- denote the upper and lower surfaces of the crack respectively. Descriptions of any remaining terms can be found in the Appendix. In the DBEM, the upper and lower surfaces

of a crack are modelled as co-planar. The displacement integral equations (equations 1 and 11) are applied to the upper surface while the traction integral equations (equations 6 and 14) are applied to the lower surface. The displacement equations are also applied to outer boundary as well. An example of this can be seen in Figure 1.

Since the fundamental solutions shown in the integral equations (2)-(4), (7)-(9), (12)-(13), (15)-(16) are of the order of $\ln(1/r)$, $1/r$, or $1/r^2$, (where r is the distance between the collocation node and the field point) mathematical singularities can occur when the collocation node lies within the same element as the field point. When dealing with weakly singular integrals with singularities of the order $\ln(1/r)$ or $1/r$ such as those seen in equations (2)-(4), (8), (9), (12)-(13), (16), the transformation of variable technique proposed by Telles [28] is used. For equations (2) and (12), rigid body motion is also applied. The strongly singular integrals with singularities of the order of $1/r^2$ seen in equations (7) and (15) only become singular when both the collocation node and the field point are on a crack surface. In many practical problems, cracks are usually modelled as piecewise flat (each individual crack element is flat), and this is the case in this work. By modelling cracks as piecewise flat, the integrals in equations (7) and (15) can be carried out analytically. For each of the integral equations seen above, when the collocation node is near to the field point, but is not in the same element as the field point, the integral shows near-singular behaviour. In this case, the element subdivision technique is used. Details on these methods can be found in [6].

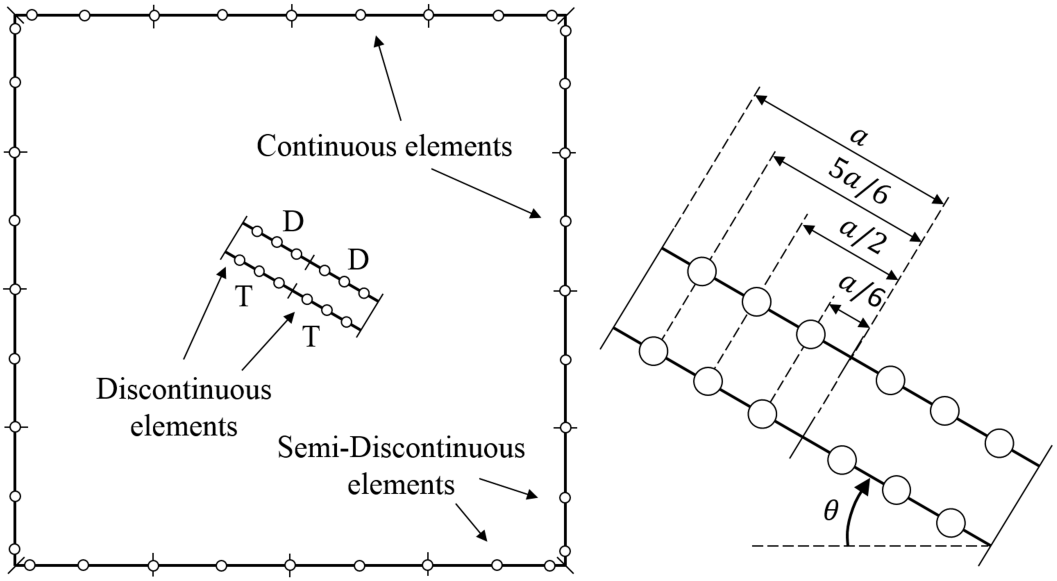

Figure 1: (Left) An example of mesh design for a square plate with a straight centre crack. Quadratic elements are used. The upper and lower surfaces of the crack are assumed to be coplanar. (Right) A zoomed-in view of the straight centre crack. The coordinates of the crack nodes can be expressed in terms of crack half-length a and crack rotation angle θ. Element end points are marked as ticks, elements nodes are marked as circles, 'D' denotes the displacement equations, and 'T' denotes the traction equations.

The system of equations used in the DBEM is of the form $\mathbf{Hu} = \mathbf{Gt}$. Where $\mathbf{H}$ and $\mathbf{G}$ are matrices of coefficients, and $\mathbf{u}$ and $\mathbf{t}$ contain boundary displacements and tractions respectively (both known and unknown). The final system of equations can be written as:

$$\mathbf{AX} = \mathbf{F} \tag{17}$$

where $\mathbf{A}$ is a matrix of coefficients, $\mathbf{X}$ is a vector of unknown boundary displacements and tractions, and $\mathbf{F}$ is a vector containing coefficients multiplied by known boundary conditions.

Cracks are discretised using discontinuous quadratic elements; continuous quadratic elements are used on the outer boundary except at the corners - where due to the non-uniqueness of the normals, semi-discontinuous quadratic elements are used. This can be seen in Figure 1.

2.2. DBEM-based IDM for Plate Bending Problems

The derivatives of the discretised DBEM integral equations for plate bending (equations 1 and 6) with respect to some geometric parameter Z_m (e.g. plate length, plate width, crack length etc.) are:

$$\frac{1}{2}w_{j,m}(\mathrm{x}^+) + \frac{1}{2}w_{j,m}(\mathrm{x}^-) + \sum_{n_e=1}^{N_e}\sum_{\gamma=1}^{M} P_{ij,m}^{b,n_e\gamma} w_j^{n_e\gamma} + \sum_{n_e=1}^{N_e}\sum_{\gamma=1}^{M} P_{ij}^{b,n_e\gamma} w_{j,m}^{n_e\gamma} \tag{18}$$
$$= \sum_{n_e=1}^{N_e}\sum_{\gamma=1}^{M} Q_{ij,m}^{b,n_e\gamma} p_j^{n_e\gamma} + \sum_{n_e=1}^{N_e}\sum_{\gamma=1}^{M} Q_{ij}^{b,n_e\gamma} p_{j,m}^{n_e\gamma} + q_3 \sum_{n_e=1}^{N_e} O_{i,m}^{b,n_e}$$

where:

$$P_{ij,m}^{b,n_e\gamma} = \neg\!\!\!\!\int_{-1}^{+1} T_{ij,m}^{b}(\mathrm{x}^+,\mathrm{x}(\eta)) N^{n_e\gamma}(\eta) J^{n_e}(\eta) d\eta + \neg\!\!\!\!\int_{-1}^{+1} T_{ij}^{b}(\mathrm{x}^+,\mathrm{x}(\eta)) N^{n_e\gamma}(\eta) J_{,m}^{n_e}(\eta) d\eta \tag{19}$$

$$Q_{ij,m}^{b,n_e\gamma} = \int_{-1}^{+1} U_{ij,m}^{b}(\mathrm{x}^+,\mathrm{x}(\eta)) N^{n_e\gamma}(\eta) J^{n_e}(\eta) d\eta + \int_{-1}^{+1} U_{ij}^{b}(\mathrm{x}^+,\mathrm{x}(\eta)) N^{n_e\gamma}(\eta) J_{,m}^{n_e}(\eta) d\eta \tag{20}$$

$$O_{i,m}^{b,n_e} = \int_{-1}^{+1} B_{i,m}^{b}(\mathrm{x}^+,\mathrm{x}(\eta)) J^{n_e}(\eta) d\eta + \int_{-1}^{+1} B_{i}^{b}(\mathrm{x}^+,\mathrm{x}(\eta)) J_{,m}^{n_e}(\eta) d\eta \tag{21}$$

where:

$$B_{i,m}^{b}(\mathrm{x}^+,\mathrm{x}) = \Big(V_{i,\alpha m}^{b}(\mathrm{x}^+,\mathrm{x}) n_\alpha(\mathrm{x}) + V_{i,\alpha}^{b}(\mathrm{x}^+,\mathrm{x}) n_{\alpha,m}(\mathrm{x})\Big) \tag{22}$$
$$- C_{11}^{b}\Big(U_{i\alpha,m}^{b}(\mathrm{x}^+,\mathrm{x}) n_\alpha(\mathrm{x}) + U_{i\alpha}^{b}(\mathrm{x}^+,\mathrm{x}) n_{\alpha,m}(\mathrm{x})\Big)$$

for the displacement integral equation, and:

$$\frac{1}{2}p_{i,m}(\mathrm{x}^-) - \frac{1}{2}p_{i,m}(\mathrm{x}^+) \tag{23}$$
$$+ n_\beta(\mathrm{x}^-)\sum_{n_e=1}^{N_e}\sum_{\gamma=1}^{M} K_{i\beta k,m}^{b,n_e\gamma} u_k^{n_e\gamma} + n_\beta(\mathrm{x}^-)\sum_{n_e=1}^{N_e}\sum_{\gamma=1}^{M} K_{i\beta k}^{b,n_e\gamma} u_{k,m}^{n_e\gamma} + n_{\beta,m}(\mathrm{x}^-)\sum_{n_e=1}^{N_e}\sum_{\gamma=1}^{M} K_{i\beta k}^{b,n_e\gamma} u_k^{n_e\gamma}$$
$$= n_\beta(\mathrm{x}^-)\sum_{n_e=1}^{N_e}\sum_{\gamma=1}^{M} L_{i\beta k,m}^{b,n_e\gamma} t_k^{n_e\gamma} + n_\beta(\mathrm{x}^-)\sum_{n_e=1}^{N_e}\sum_{\gamma=1}^{M} L_{i\beta k}^{b,n_e\gamma} t_{k,m}^{n_e\gamma} + n_{\beta,m}(\mathrm{x}^-)\sum_{n_e=1}^{N_e}\sum_{\gamma=1}^{M} L_{i\beta k}^{b,n_e\gamma} t_k^{n_e\gamma}$$
$$+ n_\beta(\mathrm{x}^-) q_3 \sum_{n_e=1}^{N_e} O_{i\beta,m}^{*,n_e} + n_{\beta,m}(\mathrm{x}^-) q_3 \left(\sum_{n_e=1}^{N_e} O_{i\beta}^{*,n_e} + \delta_{i\beta}\frac{\nu}{(1-\nu)\lambda^2}\right)$$

where:

$$K_{i\beta k,m}^{n_e\gamma} = \neg\!\!\!\!\int_{-1}^{+1} S_{i\beta k,m}^{b}(\mathrm{x}',\mathrm{x}(\eta)) N^{n_e\gamma}(\eta) J^{n_e}(\eta) d\eta + \neg\!\!\!\!\int_{-1}^{+1} S_{i\beta k}^{b}(\mathrm{x}',\mathrm{x}(\eta)) N^{n_e\gamma}(\eta) J_{,m}^{n_e}(\eta) d\eta \tag{24}$$

$$L_{i\beta k,m}^{n_e\gamma} = \neg\!\!\!\!\int_{-1}^{+1} D_{i\beta k,m}^{b}(\mathrm{x}',\mathrm{x}(\eta)) N^{n_e\gamma}(\eta) J^{n_e}(\eta) d\eta + \neg\!\!\!\!\int_{-1}^{+1} D_{i\beta k}^{b}(\mathrm{x}',\mathrm{x}(\eta)) N^{n_e\gamma}(\eta) J_{,m}^{n_e}(\eta) d\eta \tag{25}$$

$$O_{i\beta,m}^{*,n_e} = \neg\!\!\!\!\int_{-1}^{+1} B_{i\beta,m}^{*}(\mathrm{x}',\mathrm{x}(\eta)) J^{n_e}(\eta) d\eta + \neg\!\!\!\!\int_{-1}^{+1} B_{i\beta}^{*}(\mathrm{x}',\mathrm{x}(\eta)) J_{,m}^{n_e}(\eta) d\eta \tag{26}$$

and:

$$B_{i\beta,m}^{*}(\mathrm{x}',\mathrm{x}) = Q_{i\beta,m}^{*}(\mathrm{x}',\mathrm{x}) - \frac{\nu}{(1-\nu)\lambda^2}\Big(D_{i\beta\rho,m}^{b}(\mathrm{x}',\mathrm{x}) n_\rho(\mathrm{x}) + D_{i\beta\rho}^{b}(\mathrm{x}',\mathrm{x}) n_{\rho,m}(\mathrm{x})\Big) \tag{27}$$

for the traction integral equation.

The derivatives of the DBEM integral equations for two-dimensional plane stress (membrane) are:

$$\frac{1}{2}u_{\beta,m}(\mathrm{x}^+) + \frac{1}{2}u_{\beta,m}(\mathrm{x}^-) + \sum_{n_e=1}^{N_e}\sum_{\gamma=1}^{M} P_{\alpha\beta,m}^{n_e\gamma} u_{\beta}^{n_e\gamma} + \sum_{n_e=1}^{N_e}\sum_{\gamma=1}^{M} P_{\alpha\beta}^{n_e\gamma} u_{\beta,m}^{n_e\gamma} = \sum_{n_e=1}^{N_e}\sum_{\gamma=1}^{M} Q_{\alpha\beta,m}^{n_e\gamma} t_{\beta}^{n_e\gamma} + \sum_{n_e=1}^{N_e}\sum_{\gamma=1}^{M} Q_{\alpha\beta}^{n_e\gamma} t_{\beta,m}^{n_e\gamma} \tag{28}$$

where:

$$P_{\alpha\beta,m}^{n_e\gamma} = \oint_{-1}^{+1} T_{\alpha\beta,m}(\mathrm{x}', \mathrm{x}(\eta)) N^{n_e\gamma}(\eta) J^{n_e}(\eta) d\eta + \oint_{-1}^{+1} T_{\alpha\beta}(\mathrm{x}', \mathrm{x}(\eta)) N^{n_e\gamma}(\eta) J_{,m}^{n_e}(\eta) d\eta \tag{29}$$

$$Q_{\alpha\beta,m}^{n_e\gamma} = \int_{-1}^{+1} U_{\alpha\beta,m}(\mathrm{x}', \mathrm{x}(\eta)) N^{n_e\gamma}(\eta) J^{n_e}(\eta) d\eta + \int_{-1}^{+1} U_{\alpha\beta}(\mathrm{x}', \mathrm{x}(\eta)) N^{n_e\gamma}(\eta) J_{,m}^{n_e}(\eta) d\eta \tag{30}$$

for the displacement integral equation, and:

$$\begin{aligned} &\frac{1}{2}t_{\alpha,m}(\mathrm{x}^-) - \frac{1}{2}t_{\alpha,m}(\mathrm{x}^+) \\ &+ n_\beta(\mathrm{x}^-) \sum_{n_e=1}^{N_e}\sum_{\gamma=1}^{M} K_{\rho\alpha\beta,m}^{n_e\gamma} u_{\rho}^{n_e\gamma} + n_\beta(\mathrm{x}^-) \sum_{n_e=1}^{N_e}\sum_{\gamma=1}^{M} K_{\rho\alpha\beta}^{n_e\gamma} u_{\rho,m}^{n_e\gamma} + n_{\beta,m}(\mathrm{x}^-) \sum_{n_e=1}^{N_e}\sum_{\gamma=1}^{M} K_{\rho\alpha\beta}^{n_e\gamma} u_{\rho}^{n_e\gamma} \\ &= n_\beta(\mathrm{x}^-) \sum_{n_e=1}^{N_e}\sum_{\gamma=1}^{M} L_{\rho\alpha\beta,m}^{n_e\gamma} t_{\rho}^{n_e\gamma} + n_\beta(\mathrm{x}^-) \sum_{n_e=1}^{N_e}\sum_{\gamma=1}^{M} L_{\rho\alpha\beta}^{n_e\gamma} t_{\rho,m}^{n_e\gamma} + n_{\beta,m}(\mathrm{x}^-) \sum_{n_e=1}^{N_e}\sum_{\gamma=1}^{M} L_{\rho\alpha\beta}^{n_e\gamma} t_{\rho}^{n_e\gamma} \end{aligned} \tag{31}$$

where:

$$K_{\rho\alpha\beta,m}^{n_e\gamma} = \oint_{-1}^{+1} S_{\rho\alpha\beta,m}(\mathrm{x}', \mathrm{x}(\eta)) N^{n_e\gamma}(\eta) J^{n_e}(\eta) d\eta + \oint_{-1}^{+1} S_{\rho\alpha\beta}(\mathrm{x}', \mathrm{x}(\eta)) N^{n_e\gamma}(\eta) J_{,m}^{n_e}(\eta) d\eta \tag{32}$$

$$L_{\rho\alpha\beta,m}^{n_e\gamma} = \oint_{-1}^{+1} D_{\rho\alpha\beta,m}(\mathrm{x}', \mathrm{x}(\eta)) N^{n_e\gamma}(\eta) J^{n_e}(\eta) d\eta + \oint_{-1}^{+1} D_{\rho\alpha\beta}(\mathrm{x}', \mathrm{x}(\eta)) N^{n_e\gamma}(\eta) J_{,m}^{n_e}(\eta) d\eta \tag{33}$$

for the traction integral equation.

In the above equations, $T_{ij,m}^b$, $U_{ij,m}^b$, $V_{i,\alpha m}^b$, $S_{i\beta k,m}^b$, $D_{i\beta k,m}^b$, and $Q_{i\beta,m}^*$ are the derivatives of the fundamental solutions for plate bending, while $T_{\alpha\beta,m}$, $U_{\alpha\beta,m}$, $S_{\alpha\beta\rho,m}$, and $D_{\alpha\beta\rho,m}$ are the derivatives of the fundamental solutions for the membrane. The expressions for these fundamental solutions have been derived for the first time in this work and can be found in the Appendix.

While the fundamental solutions for the membrane and plate bending seen in section 2.1 are functions of the distance r between the collocation node and the field point, the derivatives of these fundamental solutions as seen in equations (18-33) are functions not only of r but also its derivative $r_{,m}$. Therefore, equations (18-33) are functions of the derivatives of the nodal coordinates. As shown in Figure 1, the coordinates of the crack nodes can be expressed in terms of the crack half-length a and crack rotation angle θ. Therefore, the derivatives of these nodal coordinates with respect to a and θ can be evaluated analytically. This is the approach taken to obtain $r_{,m}$ with the IDM.

In DBEM-based IDM the system of equations is $\mathbf{H}_{,m}\mathbf{u} + \mathbf{H}\mathbf{u}_{,m} = \mathbf{G}_{,m}\mathbf{t} + \mathbf{G}\mathbf{t}_{,m}$, where $\mathbf{H}$, $\mathbf{G}$, $\mathbf{u}$, and $\mathbf{t}$ are the same as defined in section 2.1, and $\mathbf{H}_{,m}$, $\mathbf{G}_{,m}$, $\mathbf{u}_{,m}$, and $\mathbf{t}_{,m}$ are their derivatives. This system of equations can be rewritten as:

$$\mathbf{A}\mathbf{X}_{,m} = \Big[\mathbf{F}_{,m} - \mathbf{A}_{,m}\mathbf{X}\Big] \tag{34}$$

where $\mathbf{A}$ and $\mathbf{X}$ can be obtained from equation (17). Since the right-hand side of equation (34) is known, LU decomposition can be used to obtain the unknown derivatives of boundary displacements and tractions $\mathbf{X}_{,m}$.

The entries of the matrix $\mathbf{A}_{,m}$ which correspond to the case where both the collocation node and the field point lie on fixed boundaries are zero. This occurs if a change in the geometric variable Z_m produces no change

in the coordinates of the nodes on this boundary. For example, consider a plate with a centre crack. If Z_m is the crack half-length a, then changing Z_m will not produce any change in the coordinates of the nodes on the outer boundary of the plate. Therefore, if both the collocation node and the field point lie on the outer boundary, then the corresponding entries in $\mathbf{A}_{,m}$ will be zero. Because of this, the entries of $\mathbf{A}_{,m}$ that correspond to collocation node - field node pairs that lie on fixed boundaries do not need to be calculated. This has the effect of significantly reducing the computational cost associated with evaluating $\mathbf{A}_{,m}$.

2.3. Stress Intensity Factor Evaluation

One of the most popular path-independent integrals for evaluating stress intensity factors is the J-integral. For plate bending, the rate of energy released per unit crack extension in the x_ρ direction is:

$$J^{b\rho} = \int_\Gamma \left[\Big(W^b - q_3 w_3 \Big) n_\rho^n - p_k w_{k,\rho} \right] d\Gamma \tag{35}$$

For two-dimensional plane stress (membrane) it is:

$$J^{m\rho} = \int_\Gamma \left[W^m n_\rho - t_\beta u_{\beta,\rho} \right] d\Gamma \tag{36}$$

where Γ is an arbitrary contour surrounding the crack tip, and W is strain energy density (strain energy per unit area). The strain energy density for plate bending is:

$$W^b = \frac{1}{2} \Big(M_{\alpha\beta} \chi_{\alpha\beta} + Q_\alpha \psi_\alpha \Big) \tag{37}$$

where $\chi_{\alpha\beta}$ are the flexural strains:

$$\chi_{\alpha\beta} = \frac{1}{2} \Big(w_{\alpha,\beta} + w_{\beta,\alpha} \Big) \tag{38}$$

and ψ_α are the transverse shear strains:

$$\psi_\alpha = w_\alpha + w_{3,\alpha} \tag{39}$$

The strain energy density for two-dimensional plane stress (membrane) is:

$$W^m = \frac{1}{2} N_{\alpha\beta} \epsilon_{\alpha\beta} \tag{40}$$

where $\epsilon_{\alpha\beta}$ are the in-plane strains:

$$\epsilon_{\alpha\beta} = \frac{1}{2} \Big(u_{\alpha,\beta} + u_{\beta,\alpha} \Big) \tag{41}$$

The derivatives of the rotations and displacements with respect to direction ρ in equations (35) and (36) ($w_{k,\rho}$ and $u_{\beta,\rho}$) can be calculated at some internal point x' that makes up the J-integral contour via the following discretised integral equations:

$$u_{\alpha,\rho}(\mathrm{x}') + \sum_{n_e=1}^{N_e} \sum_{\gamma=1}^{M} P_{\alpha\beta,\rho}^{n_e\gamma} u_\beta^{n_e\gamma} = \sum_{n_e=1}^{N_e} \sum_{\gamma=1}^{M} Q_{\alpha\beta,\rho}^{n_e\gamma} t_\beta^{n_e\gamma} \tag{42}$$

where:

$$Q_{\alpha\beta,\rho}^{n_e\gamma} = \int_{-1}^{+1} U_{\alpha\beta,\rho}(\mathrm{x}', \mathrm{x}(\eta)) N^{n_e\gamma}(\eta) J^{n_e}(\eta) d\eta \tag{43}$$

$$P_{\alpha\beta,\rho}^{n_e\gamma} = \int_{-1}^{+1} T_{\alpha\beta,\rho}(\mathrm{x}', \mathrm{x}(\eta)) N^{n_e\gamma}(\eta) J^{n_e}(\eta) d\eta \tag{44}$$

for the membrane, and:

$$w_{i,\rho}(\mathrm{x}') + \sum_{n_e=1}^{N_e} \sum_{\gamma=1}^{M} P_{ij,\rho}^{b,n_e\gamma} w_j^{n_e\gamma} = \sum_{n_e=1}^{N_e} \sum_{\gamma=1}^{M} Q_{ij,\rho}^{b,n_e\gamma} p_j^{n_e\gamma} + q_3 \sum_{n_e=1}^{N_e} O_{i,\rho}^{b,n_e} \tag{45}$$

where:

$$Q_{ij,\rho}^{b,n_e\gamma} = \int_{-1}^{+1} U_{ij,\rho}^{b}(\mathrm{x}', \mathrm{x}(\eta)) N^{n_e\gamma}(\eta) J^{n_e}(\eta) d\eta \tag{46}$$

$$P_{ij,\rho}^{b,n_e\gamma} = \int_{-1}^{+1} T_{ij,\rho}^{b}(\mathrm{x}', \mathrm{x}(\eta)) N^{n_e\gamma}(\eta) J^{n_e}(\eta) d\eta \tag{47}$$

$$O_{i,\rho}^{b,n_e} = \int_{-1}^{+1} B_{i,\rho}^{b}(\mathrm{x}', \mathrm{x}(\eta)) J^{n_e}(\eta) d\eta \tag{48}$$

and:

$$B_{i,\rho}^{b}(\mathrm{x}', \mathrm{x}) = V_{i,\alpha\rho}^{b}(\mathrm{x}', \mathrm{x}) n_\alpha(\mathrm{x}) - \frac{\nu}{(1-\nu)\lambda^2} U_{i\alpha,\rho}^{b}(\mathrm{x}', \mathrm{x}) n_\alpha(\mathrm{x}) \tag{49}$$

for plate bending. Expressions for the fundamental solutions $U_{\alpha\beta,\rho}$, $T_{\alpha\beta,\rho}$, $U_{ij,\rho}^{b}$, $T_{ij,\rho}^{b}$, and $V_{i,\alpha\rho}^{b}$ can be found in [6].

The fundamental solutions $U_{\alpha\beta,\rho}$, $T_{\alpha\beta,\rho}$, $U_{ij,\rho}^{b}$, $T_{ij,\rho}^{b}$, and $V_{i,\alpha\rho}^{b}$ are the derivatives with respect to direction ρ of the fundamental solutions introduced in section 2.1.

The component of the plate-bending J-integral in the x_1 direction is related to the bending stress intensity factors for fracture modes I, II, and III in the following manner:

$$J^{b1} = \frac{12}{Eh^3}\left[(K_I^b)^2 + (K_{II}^b)^2 + \frac{h^2(1+\nu)}{10}(K_{III}^b)^2\right] \tag{50}$$

Likewise, the component of the membrane J-integral in the x_1 direction is related to the membrane stress intensity factors for modes I and II in the following manner:

$$J^{m1} = \frac{(K_I^m)^2 + (K_{II}^m)^2}{E'h} \tag{51}$$

where E' is Young's modulus, it is equal to E in the case of plane stress, or $E/(1-\nu^2)$ in the case of plane strain. In order to obtain the individual stress intensity factors, the J-integral needs to be decoupled. A method of achieving this for the membrane was presented in [12], a similar procedure for plate bending was presented by Dirgantara and Aliabadi [7]. The membrane and plate-bending J-integrals can be decoupled into symmetric J_S and anti-symmetric J_{AS} components:

$$J^{m1} = J_S^{m1} + J_{AS}^{m1} \qquad J^{b1} = J_S^{b1} + J_{AS}^{b1} \tag{52}$$

where:

$$J_S^{m1} = J_I^{m1} = \frac{(K_I^m)^2}{E'h} \qquad J_{AS}^{m1} = J_{II}^{m1} = \frac{(K_{II}^m)^2}{E'h} \tag{53}$$

and:

$$J_S^{b1} = J_I^{b1} = \frac{12}{Eh^3}(K_I^b)^2 \qquad J_{AS}^{b1} = J_{II}^{b1} + J_{III}^{b1} = \frac{12}{Eh^3}\left[(K_{II}^b)^2 + \frac{h^2(1+\nu)}{10}(K_{III}^b)^2\right] \tag{54}$$

Therefore, the individual stress intensity factors for the membrane can be written as:

$$K_I^m = \sqrt{\frac{J_I^{1m} E'h}{(1-\nu^2)}} \tag{55}$$

$$K_{II}^m = \sqrt{\frac{J_{II}^{1m} E'h}{(1-\nu^2)}} \tag{56}$$

To split the mode II and mode III components of J_{AS}^{b1}, a displacement ratio as proposed by Rigby and Aliabadi [29] is used:

$$\Delta w_1 = w_{1(+180^\circ)} - w_{1(-180^\circ)} = \frac{48}{Eh^3}\sqrt{2r} K_{II}^b \tag{57}$$

$$\Delta w_3 = w_{3(+180^\circ)} - w_{3(-180^\circ)} = \frac{24(1+\nu)}{5Eh}\sqrt{2r}K_{III}^b \tag{58}$$

$$\frac{\Delta w_1}{\Delta w_3} = \frac{10}{(1+\nu)h^2}\frac{K_{II}^b}{K_{III}^b} \tag{59}$$

where the subscripts (-180°) and $(+180^\circ)$ denote that the values were calculated on the lower and upper surfaces of the crack respectively.

By substituting equation (59) into equation (54) the plate bending stress intensity factors for modes II and III can be obtained:

$$K_I^b = \sqrt{\frac{Eh^3}{12}J_I^{1b}} \tag{60}$$

$$K_{II}^b = \sqrt{\frac{J_{II}^{1b}}{\frac{12}{Eh^3}\left[1+\frac{10}{(1+\nu)h^2}\left(\frac{\Delta w_3}{\Delta w_1}\right)^2\right]}} \tag{61}$$

$$K_{III}^b = \sqrt{\frac{J_{II}^{1b}}{\frac{12(1+\nu)}{10Eh}\left[1+\frac{(1+\nu)h^2}{10}\left(\frac{\Delta w_1}{\Delta w_3}\right)^2\right]}} \tag{62}$$

The maximum values of the stress intensity factors through the thickness of the plate are:

$$K_I^{max} = \frac{K_I^m}{h} + \frac{6}{h^2}K_I^b \tag{63}$$

$$K_{II}^{max} = \frac{K_{II}^m}{h} + \frac{6}{h^2}K_{II}^b \tag{64}$$

$$K_{III}^{max} = \frac{3}{2h}K_{III}^b \tag{65}$$

Regarding the implementation of the J-integral using the DBEM - the J-integral path can be chosen as a circular path centred around the crack tip. A series of equidistant internal points make up the circular path. The integrations seen in equations (35) and (36) are carried out over this path using the simple Trapezoidal rule. The cracks in this work are assumed to be traction-free, therefore the contribution of the integration over the crack surfaces included in the contour is equal to zero. Therefore, the circular path is the only component of the contour. Various integration paths starting from different crack nodes can be seen in Figure 2. The different integration paths were found to provide similar results, although it was found that the results gradually converged as the starting node moved further from the crack tip. The results typically converged after the 5th node, with the results from $S5$ and $S7$ showing very little difference.

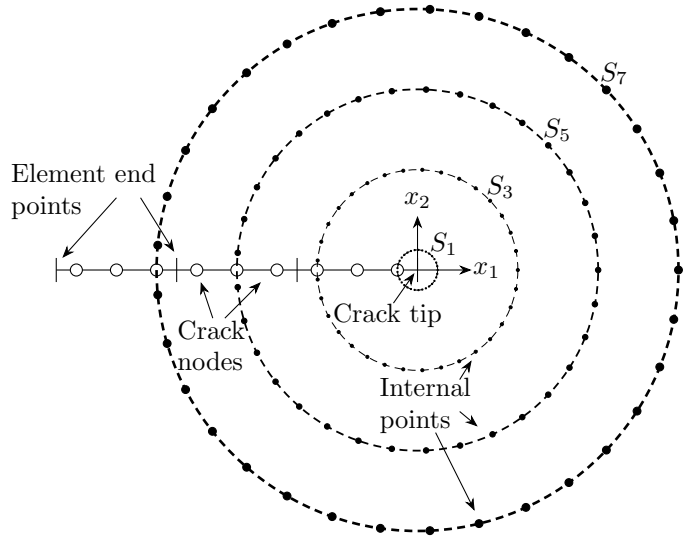

Figure 2: The integration paths around a crack tip used to evaluate the J-integral. 32 internal points symmetric about the crack axis are present along each integration path. The paths are named according to the crack node each path starts from.

2.4. Stress Intensity Factor Sensitivity Evaluation

The derivative of the J-integral for plate bending with respect to some geometric variable Z_m can be obtained from equation (35):

$$J^{b\rho}_{,m} = \int_\Gamma \left[\Big(W^b_{,m} - q_3 w_{3,m} \Big) n^n_\rho + \Big(W^b - q_3 w_3 \Big) n^n_{\rho,m} - p_k w_{k,\rho m} \right] d\Gamma + \int_\Gamma \left[\Big(W^b - q_3 w_3 \Big) n^n_\rho - p_k w_{k,\rho} \right] (d\Gamma)_{,m} \quad (66)$$

Likewise for two-dimensional plane stress (membrane):

$$J^{m\rho}_{,m} = \int_\Gamma \left[\Big(W^m_{,m} n_\rho + W^m n_{\rho,m} \Big) - \Big(t_{\beta,m} u_{\beta,\rho} + t_\beta u_{\beta,\rho m} \Big) \right] d\Gamma + \int_\Gamma \left[W^m n_\rho - t_\beta u_{\beta,\rho} \right] (d\Gamma)_{,m} \quad (67)$$

where the strain energy density derivatives for plate bending and membrane are:

$$W^b_{,m} = \frac{1}{2} \Bigg(M_{\alpha\beta,m} \chi_{\alpha\beta} + M_{\alpha\beta} \chi_{\alpha\beta,m} + Q_{\alpha,m} \psi_\alpha + Q_\alpha \psi_{\alpha,m} \Bigg) \quad (68)$$

and:

$$W^m_{,m} = \frac{1}{2} \Big(N_{\alpha\beta,m} \epsilon_{\alpha\beta} + N_{\alpha\beta} \epsilon_{\alpha\beta,m} \Big) \quad (69)$$

respectively.

Similar to the method shown in section 2.3, the derivatives of the rotation sensitivities and displacement sensitivities with respect to direction ρ in equations (66) and (67) ($w_{k,\rho m}$ and $u_{\beta,\rho m}$) can be calculated at some internal point x' that makes up the J-integral contour via the following integral equations:

$$u_{\alpha,\rho m}(\mathrm{x}') + \sum_{n_e=1}^{N_e} \sum_{\gamma=1}^{M} P^{n_e\gamma}_{\alpha\beta,\rho m} u^{n_e\gamma}_\beta + \sum_{n_e=1}^{N_e} \sum_{\gamma=1}^{M} P^{n_e\gamma}_{\alpha\beta,\rho} u^{n_e\gamma}_{\beta,m} = \sum_{n_e=1}^{N_e} \sum_{\gamma=1}^{M} Q^{n_e\gamma}_{\alpha\beta,\rho m} t^{n_e\gamma}_\beta + \sum_{n_e=1}^{N_e} \sum_{\gamma=1}^{M} Q^{n_e\gamma}_{\alpha\beta,\rho} t^{n_e\gamma}_{\beta,m} \quad (70)$$

where:

$$P^{n_e\gamma}_{\alpha\beta,\rho m} = \fint_{-1}^{+1} T_{\alpha\beta,\rho m}(\mathrm{x}', \mathrm{x}(\eta)) N^{n_e\gamma}(\eta) J^{n_e}(\eta) d\eta + \fint_{-1}^{+1} T_{\alpha\beta,\rho}(\mathrm{x}', \mathrm{x}(\eta)) N^{n_e\gamma}(\eta) J^{n_e}_{,m}(\eta) d\eta \quad (71)$$

$$Q^{n_e\gamma}_{\alpha\beta,\rho m} = \int_{-1}^{+1} U_{\alpha\beta,\rho m}(\mathrm{x}', \mathrm{x}(\eta)) N^{n_e\gamma}(\eta) J^{n_e}(\eta) d\eta + \int_{-1}^{+1} U_{\alpha\beta,\rho}(\mathrm{x}', \mathrm{x}(\eta)) N^{n_e\gamma}(\eta) J^{n_e}_{,m}(\eta) d\eta \quad (72)$$

for the membrane, and:

$$\begin{aligned} & w_{j,\rho m}(\mathrm{x}') + \sum_{n_e=1}^{N_e} \sum_{\gamma=1}^{M} P^{b,n_e\gamma}_{ij,\rho m} w^{n_e\gamma}_j + \sum_{n_e=1}^{N_e} \sum_{\gamma=1}^{M} P^{b,n_e\gamma}_{ij,\rho} w^{n_e\gamma}_{j,m} \\ & = \sum_{n_e=1}^{N_e} \sum_{\gamma=1}^{M} Q^{b,n_e\gamma}_{ij,\rho m} p^{n_e\gamma}_j + \sum_{n_e=1}^{N_e} \sum_{\gamma=1}^{M} Q^{b,n_e\gamma}_{ij,\rho} p^{n_e\gamma}_{j,m} + q_3 \sum_{n_e=1}^{N_e} O^{n,n_e}_{i,\rho m} \end{aligned} \quad (73)$$

where:

$$P^{b,n_e\gamma}_{ij,\rho m} = \fint_{-1}^{+1} T^b_{ij,\rho m}(\mathrm{x}', \mathrm{x}(\eta)) N^{n_e\gamma}(\eta) J^{n_e}(\eta) d\eta + \fint_{-1}^{+1} T^b_{ij,\rho}(\mathrm{x}', \mathrm{x}(\eta)) N^{n_e\gamma}(\eta) J^{n_e}_{,m}(\eta) d\eta \quad (74)$$

$$Q^{b,n_e\gamma}_{ij,\rho m} = \int_{-1}^{+1} U^b_{ij,\rho m}(\mathrm{x}', \mathrm{x}(\eta)) N^{n_e\gamma}(\eta) J^{n_e}(\eta) d\eta + \int_{-1}^{+1} U^b_{ij,\rho}(\mathrm{x}', \mathrm{x}(\eta)) N^{n_e\gamma}(\eta) J^{n_e}_{,m}(\eta) d\eta \quad (75)$$

$$O^{b,n_e\gamma}_{i,\rho m} = \int_{-1}^{+1} B^b_{i,\rho m}(\mathrm{x}', \mathrm{x}(\eta)) J^{n_e}(\eta) d\eta + \int_{-1}^{+1} B^b_{i,\rho}(\mathrm{x}', \mathrm{x}(\eta)) J^{n_e}_{,m}(\eta) d\eta \quad (76)$$

where:

$$\begin{aligned} B^b_{i,\rho m}(\mathrm{x}', \mathrm{x}) = & \Big(V^b_{i,\alpha\rho m}(\mathrm{x}', \mathrm{x}) n_\alpha(\mathrm{x}) + V^b_{i,\alpha\rho}(\mathrm{x}', \mathrm{x}) n_{\alpha,m}(\mathrm{x}) \Big) \\ & - \frac{\nu}{(1-\nu)\lambda^2} \Big(U^b_{i\alpha,\rho m}(\mathrm{x}', \mathrm{x}) n_\alpha(\mathrm{x}) + U^b_{i\alpha,\rho}(\mathrm{x}', \mathrm{x}) n_{\alpha,m}(\mathrm{x}) \Big) \end{aligned} \quad (77)$$

for plate bending. Expressions for the fundamental solutions $T_{\alpha\beta,\rho m}$, $U_{\alpha\beta,\rho m}$, $T^b_{ij,\rho m}$, $U^b_{ij,\rho m}$, and $V^b_{i,\alpha\rho m}$ can be found in the Appendix.

The fundamental solutions $U_{\alpha\beta,\rho m}$, $T_{\alpha\beta,\rho m}$, $U^b_{ij,\rho m}$, $T^b_{ij,\rho m}$, and $V^b_{i,\alpha\rho m}$ are the derivatives with respect to direction ρ of the fundamental solutions introduced in section 2.2.

The individual mode components of $J^{m1}_{,m}$ and $J^{b1}_{,m}$ can be decoupled by using a similar procedure to that shown in section 2.3. Therefore, the sensitivities of the individual stress intensity factors for the membrane can be written as:

$$K^m_{I,m} = \frac{J^{1m}_{I,m}}{2K^m_I}\frac{E}{(1-\nu^2)} \tag{78}$$

$$K^m_{II,m} = \frac{J^{1m}_{II,m}}{2K^m_{II}}\frac{E}{(1-\nu^2)} \tag{79}$$

The sensitivities of the plate bending stress intensity factors for modes I, II, and III are:

$$K^b_{I,m} = \frac{Eh^3 J^b_{I,m}}{24K^b_I} \tag{80}$$

$$K^b_{II,m} = \frac{Eh^3}{24K^b_{II}\left(1+\frac{10}{(1+\nu)h^2}\left(\frac{\Delta w_3}{\Delta w_1}\right)^2\right)^2}\left\{J^b_{II,m}\left(1+\frac{10}{(1+\nu)h^2}\left(\frac{\Delta w_3}{\Delta w_1}\right)^2\right) - \frac{20}{(1+\nu)h^2}J^b_{II}\left(\frac{\Delta w_3}{\Delta w_1}\right)\left(\frac{\Delta w_3}{\Delta w_1}\right)_{,m}\right\} \tag{81}$$

$$K^b_{III,m} = \frac{5Eh}{12(1+\nu)K^b_{III}\left(1+\frac{(1+\nu)h^2}{10}\left(\frac{\Delta w_3}{\Delta w_1}\right)^{-2}\right)^2}\left\{J^b_{II,m}\left(1+\frac{(1+\nu)h^2}{10}\left(\frac{\Delta w_3}{\Delta w_1}\right)^{-2}\right) + 2J^b_{II}\frac{(1+\nu)h^2}{10}\left(\frac{\Delta w_3}{\Delta w_1}\right)^{-3}\left(\frac{\Delta w_3}{\Delta w_1}\right)_{,m}\right\} \tag{82}$$

The sensitivities of the maximum values of the stress intensity factors through the thickness of the plate are:

$$K^{max}_{I,m} = \frac{K^m_{I,m}}{h} + \frac{6}{h^2}K^b_{I,m} \tag{83}$$

$$K^{max}_{II,m} = \frac{K^m_{II,m}}{h} + \frac{6}{h^2}K^b_{II,m} \tag{84}$$

$$K^{max}_{III,m} = \frac{3}{2h}K^b_{III,m} \tag{85}$$

2.5. DBEM-based FDM for Plate Bending Problems

For the DBEM-based FDM, the first-order central finite difference scheme is used to obtain the sensitivities of a stress intensity factor K with respect to a change in some geometric variable Z_m:

$$\frac{\partial K(Z_m)}{\partial Z_m} = K_{,m} = \frac{K(Z_m+\Delta Z_m) - K(Z_m-\Delta Z_m)}{2\Delta Z_m} \tag{86}$$

where ΔZ_m is the step size. The choice of ΔZ_m has significant influence on the accuracy of the derivative $K_{,m}$, if ΔZ_m is too small then there will be significant rounding error, and if ΔZ_m is too large then there will be significant truncation error [30]. Since the optimal step size will change depending on the value of Z_m, a normalised step size $\Delta Z'_m$ is used such that $\Delta Z_m = Z_m \Delta Z'_m$. In this work, an optimisation procedure is carried out to determine the optimal normalised step size $\Delta Z'_m$.

2.6. First-Order Reliability Method (FORM)

In the field of structural reliability analysis, the boundary between the structure failing and not-failing is defined as a 'limit state'. This can be represented mathematically as a limit state function (LSF) or performance function $g(\mathbf{Z})$ [5]:

$$g(\mathbf{Z}) = R - S(\mathbf{X}) \tag{87}$$

where R is the resistance of the structure to some load effect S, $\mathbf{Z}$ is a size q vector containing all of the design variables that influence g, and $\mathbf{X}$ ($\mathbf{X} \subseteq \mathbf{Z}$) is a size n ($n = q - 1$) vector of the design variables that influence S.

The reliability, P_R, of a structure can be determined by evaluating the following integral:

$$P_R = 1 - P_F = P\{g(\mathbf{Z}) > 0\} = \int\limits_{g(\mathbf{Z})>0} f_{\mathbf{Z}}(\mathbf{Z}) d\mathbf{Z} \tag{88}$$

where $f_{\mathbf{Z}}(\mathbf{Z})$ is the joint PDF of $\mathbf{Z}$. P_F and P_R involve integrating $f_{\mathbf{Z}}(\mathbf{Z})$ over the regions defined by $g(\mathbf{Z}) < 0$ (the failure region) and $g(\mathbf{Z}) > 0$ (the safe region) respectively. All of the design variables are assumed to be mutually independent. The direct evaluation of the above integral is usually very difficult since it can be multidimensional if many design variables are involved. The integration boundary $g(\mathbf{Z}) = 0$ can also be multidimensional and is usually a non-linear function.

The First-Order Reliability Method (FORM) is a method that can be used to evaluate this integral and is used in this work for this purpose. The version of FORM used in this work is the Advanced First-Order Second-Moment (AFOSM) method for non-linear limit sate functions. More details on this method, and on structural reliability analysis in general, can be found in [31].

3. Numerical Example

A numerical example involving a thick plate with an inclined centre crack subjected to membrane, bending, and pressure loads is investigated. The plate used in this example can be seen in Figure 3. The plate is made from steel, and is modelled using 32 quadratic elements on the outer boundary (8 for each edge), and 48 quadratic elements on the crack (24 for each crack face).

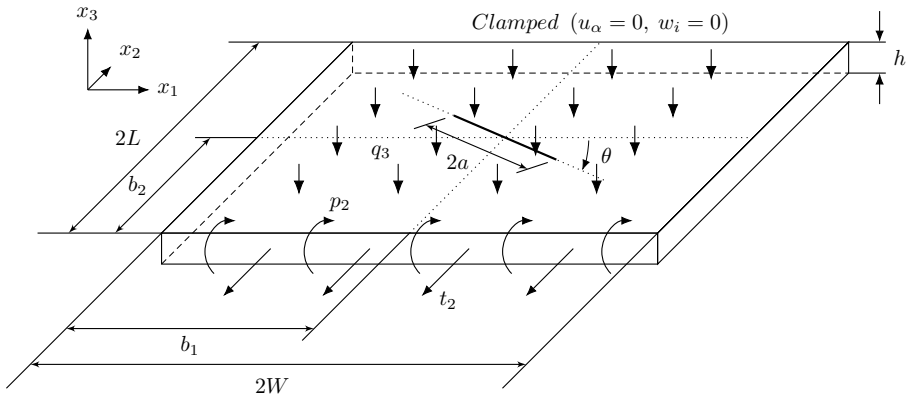

Figure 3: Thick plate with an inclined through-thickness crack. The plate is subjected to the combined loading of a membrane traction, a bending moment, and a uniform load. The geometric variables b_1 and b_2 denote the offset of the centre of the crack in the x_1 and x_2 directions respectively from the low-left corner of the plate.

This example is split into two parts. In the first part, the SIF sensitivities of the critical crack tip are calculated using the DBEM-based IDM (DBEM-IDM) and the DBEM-based FDM (DBEM-FDM). The purpose

of this first part is to demonstrate the superior robustness and efficiency of the DBEM-IDM when compared to the DBEM-FDM. In the second part, reliability analyses are carried out with the FORM using the SIF sensitivities from the DBEM-IDM. The purpose of this second part is to demonstrate one possible application of the SIF sensitivities calculated from the DBEM-IDM.

3.1. Stress Intensity Factor Sensitivities

The values of the geometric and loading design variables used in this first part of the example can be seen in Table 1.

Table 1: The design variables used in the first part of the numerical example.

Parameter	Description	Value
θ	Crack rotation angle	30° (0.524 rad)
a	Crack half-length	Variable (from 0.1-0.8 m)
b_1	x_1 position of the crack	1 m
b_2	x_2 position of the crack	1 m
L	Plate half-length	1 m
W	Plate half-width	1 m
h	Plate thickness	0.15 m
t_2	Membrane traction	4 MNm^{-1}
p_2	Bending moment	5 MN
q_3	Uniform load	2 MNm^{-2}
E	Young's modulus	206.8 GNm^{-2}
ν	Poisson's ratio	0.29

The sensitivities of the maximum SIFs through the thickness of the plate (equations 83-85) with respect to crack half-length a were calculated using both the DBEM-FDM and the DBEM-IDM with the J-integral. The J-integral path used was the 5th path (S5 in Figure 2), and 32 internal points were used on this path. It was found from a convergence study that increasing the path number or the number of internal points above these values did not produce much change in the SIF sensitivities. The optimal normalised step size for the DBEM-FDM was found to vary depending on the value of a/L. The procedure to find the optimal normalised step size for a particular value of a/L involved calculating these sensitivities for a wide range of values of $\Delta Z'_m$ from 1×10^{-5} to 9×10^{-1}. There will be a range of values of $\Delta Z'_m$ for which the sensitivities are stable, and the optimal value of $\Delta Z'_m$ is chosen from this range. It was found that a value of $\Delta Z'_m = 8 \times 10^{-2}$ provided sufficiently stable sensitivities at all of the values of a/L investigated. As mentioned in section 2.1, the DBEM-IDM involves evaluating the nodal coordinate derivatives analytically. It therefore avoids the time-consuming optimisation procedure required for the DBEM-FDM.

The normalised maximum stress intensity factors and their sensitivities can be seen in Figures 4 and 5 respectively. It can be seen that the sensitivities from the DBEM-FDM and the DBEM-IDM compared well for all three maximum SIFs. Based on the data in the three sub-Figures of Figure 5, the mean absolute percentage difference between the DBEM-FDM and the DBEM-IDM was 2.28%, 3.22%, and 2.37% for the sensitivities of K_I^{max}, K_{II}^{max}, and K_{III}^{max} respectively. These represent very small differences. In Figure 5c it can be seen that there is a large difference of about 11.62% between the DBEM-FDM and the DBEM-IDM at $a/L = 0.15$. This can be explained by the observation that at relatively small crack sizes ($a/L \leq 0.2$) there is only a small range of values of $\Delta Z'_m$ for which the SIF sensitivities are stable. This complicates the procedure of determining the optimal value of $\Delta Z'_m$.

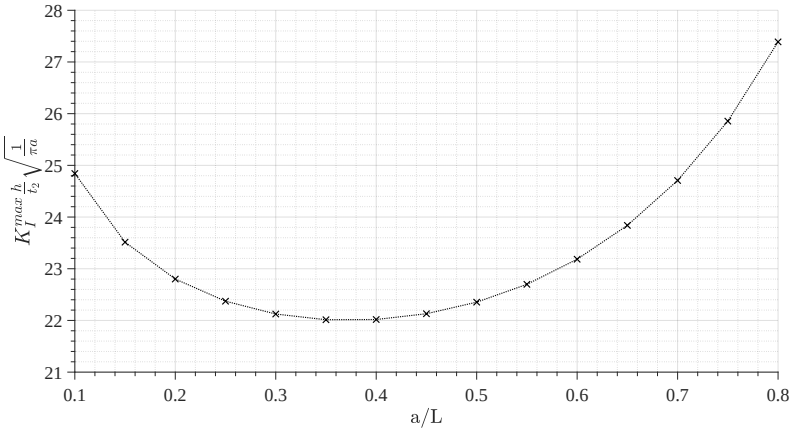

(a)

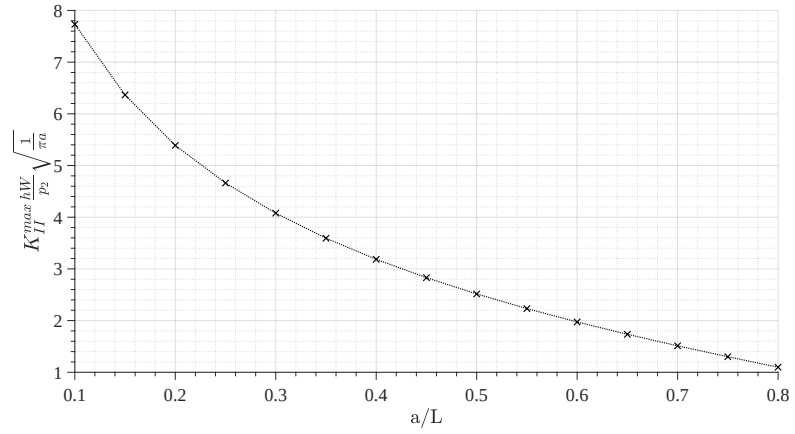

(b)

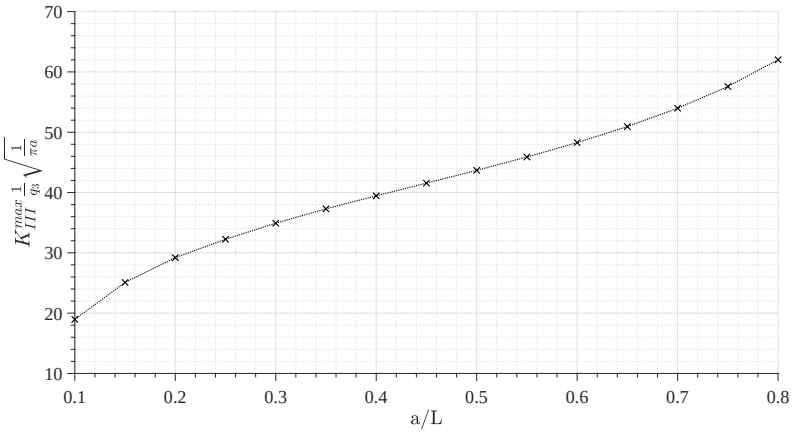

(c)

Figure 4: Normalised maximum stress intensity factors obtained from the DBEM from the J-integral using path S_5 (see Figure 2). These stress intensity factors were evaluated at $\theta = 30°$ (0.52 rads). (a) K_I^{max}, (b) K_{II}^{max}, (c) K_{III}^{max}.

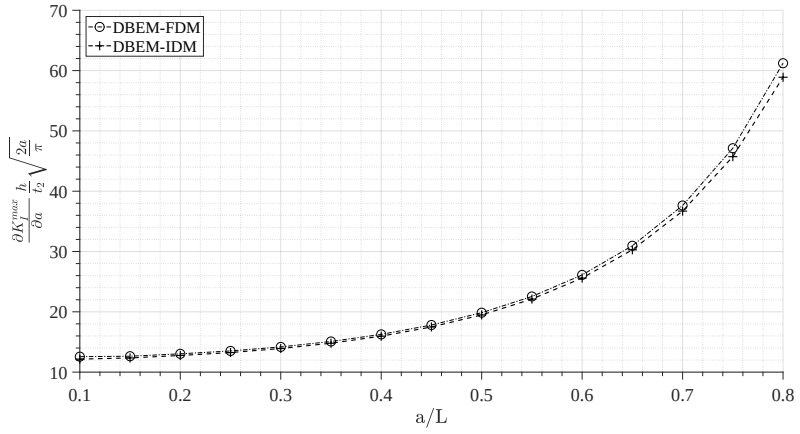

(a)

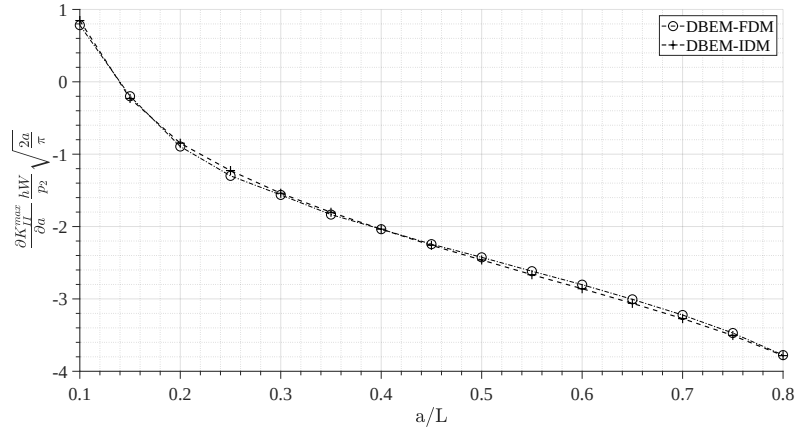

(b)

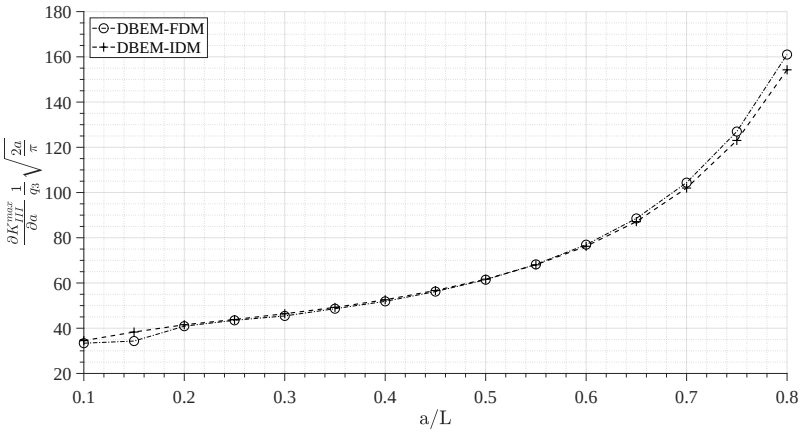

(c)

Figure 5: Normalised maximum stress intensity factor sensitivities obtained from the DBEM-FDM and the DBEM-IDM from the J-integral using path S_5 (see Figure 2) with respect to crack half-length a vs. a/L. These sensitivities were evaluated at $\theta = 30°$ (0.52 rads). The normalised stepsize used for the DBEM-FDM is 5×10^{-2}. (a) K_I^{max}, (b) K_{II}^{max}, (c) K_{III}^{max}.

A convergence study of the SIF sensitivities from the DBEM-IDM was performed with respect to the J-integral path used and the number of internal points making up the J-integral path. The results of this study can be seen in Figure 6. It can be seen that the SIF sensitivities for paths S_4-S_6 are very similar. The SIF sensitivities from S_4 showed a maximum percentage difference with respect to those from S_6 of only 2.17%. This small difference indicates the SIF sensitivities are largely insensitive to the J-integral path used. It can also be seen that the SIF sensitivities for each path converge as the number of internal points is increased. Based

on these results, the J-integral path and the number of internal points on this path were chosen as S_5 and 32 respectively.

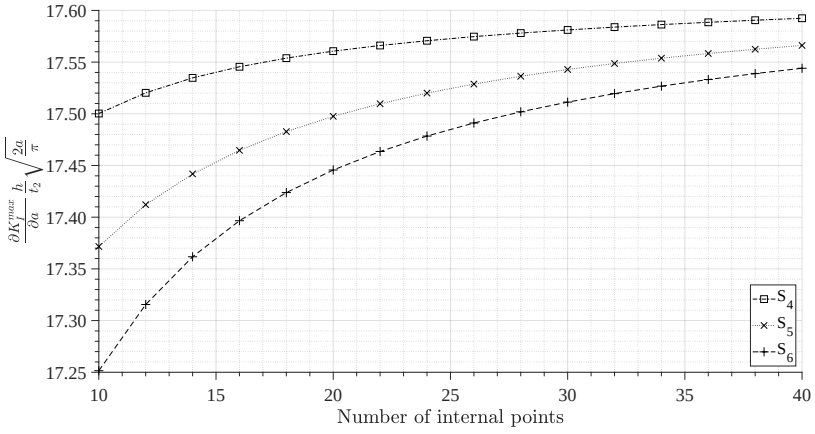

(a)

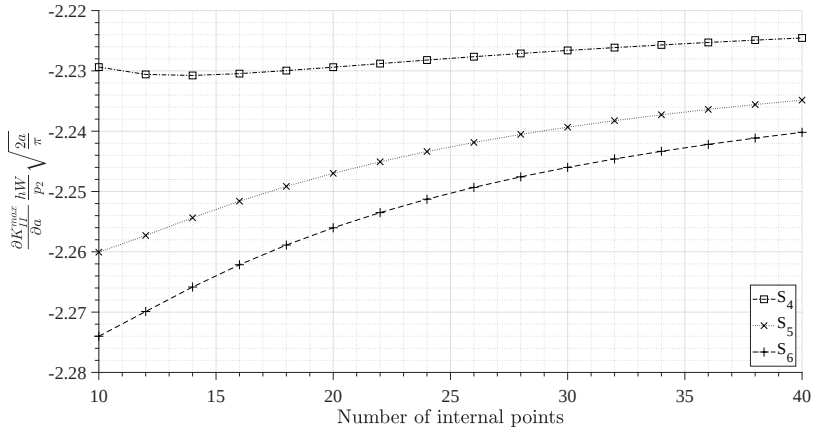

(b)

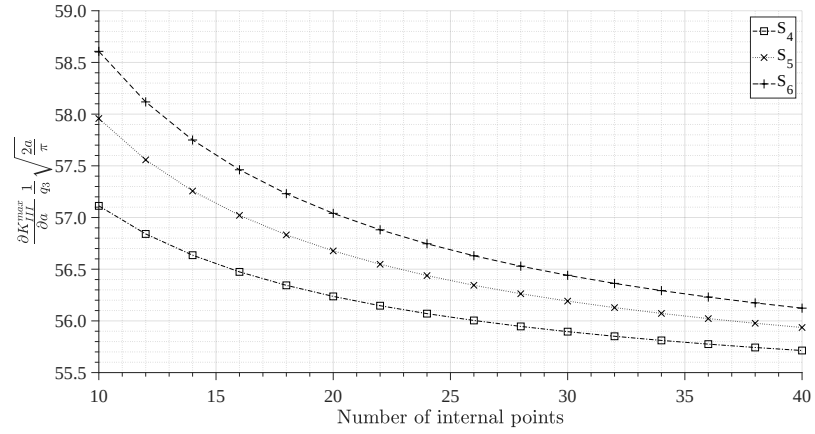

(c)

Figure 6: Normalised maximum stress intensity factor sensitivities obtained from the DBEM-IDM from the J-integral using paths S_4-S_6 (see Figure 2) with respect to crack half-length a vs. the number of internal points used on each path. These sensitivities were evaluated at $a/L = 0.45$ and $\theta = 30°$ (0.52 rads). (a) K_I^{max}, (b) K_{II}^{max}, (c) K_{III}^{max}.

A convergence study of the SIF sensitivities from the DBEM-IDM was also performed with respect to the number of elements on each of the two crack faces. The results are presented in Figure 7. It can be seen that the SIF sensitivities tend to converge as the number of elements on each crack face is increased. The SIF sensitivities calculated with 24 or 28 elements show absolute percentage differences with those calculated

with 32 elements of, at most, only 3.45% and 1.18% respectively. Because of these small differences, and also to reduce computation time, 24 elements were used on each crack face in this work. The SIFs and their sensitivities proved to be very insensitive to the number of elements on the outer boundary. It was decided to use 8 elements per edge on the outer boundary to reduce computation time.

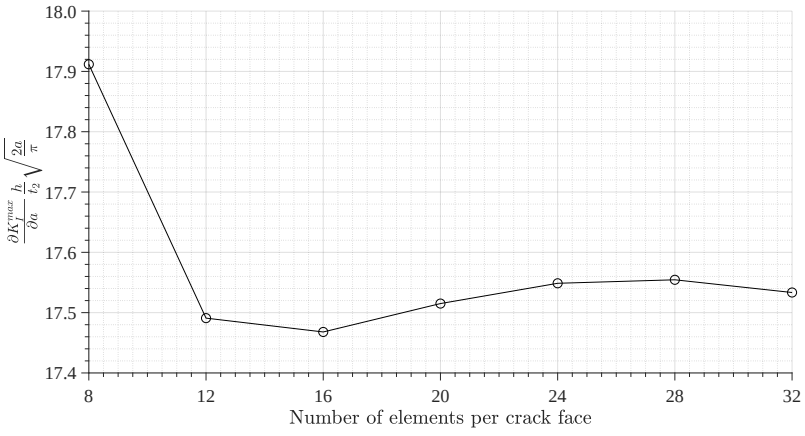

(a)

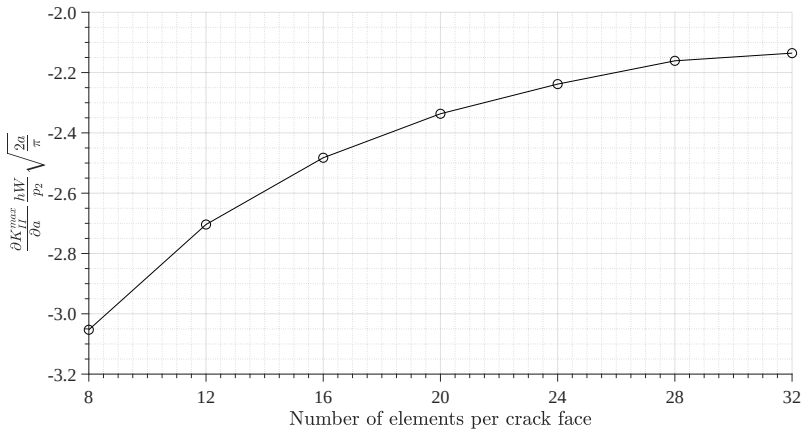

(b)

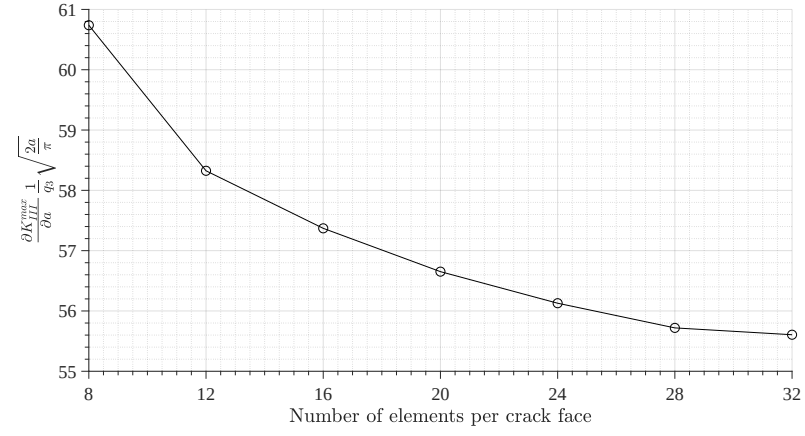

(c)

Figure 7: Normalised maximum stress intensity factor sensitivities obtained from the DBEM-IDM from the J-integral using path S_5 (see Figure 2) with respect to crack half-length a vs. the number elements used on each crack surface. These sensitivities were evaluated at $a/L = 0.45$ and $\theta = 30^\circ$ (0.52 rads). (a) K_I^{max}, (b) K_{II}^{max}, (c) K_{III}^{max}.

3.2. Reliability Analysis

In this second part of the numerical example, reliability analyses are carried out on the plate seen in Figure 3. The failure condition of this plate is with regards to the onset of crack growth. The limit state function g in this case is:

$$g(\mathbf{Z}) = G_o - G_{eff}(\mathbf{X}) \tag{89}$$

where G_o is the strain energy release rate required for the onset of crack growth, and G_{eff} is the effective strain energy release rate at the critical crack tip. The vector $\mathbf{Z}$ is composed of design variables that influence g: $\mathbf{Z} = (\theta, a, b_1, b_2, L, W, h, t_2, p_2, q_3, E, \nu, G_o)$, while the vector $\mathbf{X}$ is composed of design variables that influence G_{eff}: $\mathbf{X} = (\theta, a, b_1, b_2, L, W, h, t_2, p_2, q_3, E, \nu)$. The distributions of these variables can be seen in Table 2. The distribution assigned to G_o should ideally be found experimentally for the particular combination of loads presented in this example. For demonstration purposes, G_o is given an arbitrary distribution.

Table 2: The design variables used in the reliability analyses conducted in the second half of the numerical example.

Z_i	X_i	Parameter	Description	Distribution	Mean μ	COV
Z_1	X_1	θ	Crack rotation angle	Normal	30° (0.524 rad)	0.05
Z_2	X_2	a	Crack half-length	Lognormal	0.1 m	0.05
Z_3	X_3	b_1	x_1 position of the crack	Lognormal	1 m	0.05
Z_4	X_4	b_2	x_2 position of the crack	Normal	1 m	0.05
Z_5	X_5	L	Plate half-length	Lognormal	1 m	0.05
Z_6	X_6	W	Plate half-width	Normal	1 m	0.05
Z_7	X_7	h	Plate thickness	Lognormal	0.15 m	0.05
Z_8	X_8	t_2	Membrane traction	Normal	4 MN/m	0.1
Z_9	X_9	p_2	Bending moment	Lognormal	5 MN	0.1
Z_{10}	X_{10}	q_3	Uniform load	Normal	2 MN/m^2	0.1
Z_{11}	X_{11}	E	Young's modulus	Lognormal	206.8 GPa	0.2
Z_{12}	X_{12}	ν	Poisson's ratio	Lognormal	0.29	0.2
Z_{13}	-	G_o	Strain energy release rate required for crack growth onset	Normal	100 J/m^2	0.2

The sensitivities of $g(\mathbf{Z})$ with respect to the variables in $\mathbf{Z}$ are required by the FORM to evaluate the probability of failure P_F. The sensitivities with respect to variables Z_1 to Z_6 can be evaluated using the DBEM-IDM since they are geometric variables. While the sensitivities with respect to the non-geometric variables Z_7 to Z_{12} can be evaluated using the DBEM-FDM. The sensitivity of $g(\mathbf{Z})$ with respect to G_o can be evaluated analytically. In this work it was found that a normalised step size of $\Delta Z'_m = 5\times10^{-2}$ provided stable sensitivities from the DBEM-FDM for variables Z_7 to Z_{12}. The nodal coordinate derivatives with respect to variables Z_1 to Z_6 required by the DBEM-IDM can be evaluated analytically.

The effective strain energy release rate G_{eff} takes into account the combined effects of membrane and bending loads. An equation for G_{eff} was proposed by Dirgantara and Aliabadi [32]. A slightly modified version of this equation, such that mode-II and mode-III components are separated from mode-I components, is used in this work:

$$G_{eff}(\mathbf{X}) = G_I^m(\mathbf{X}) + T_I G_I^b(\mathbf{X}) + T_{II}\Big(G_{II}^m(\mathbf{X}) + G_{II}^b(\mathbf{X}) + G_{III}^b(\mathbf{X})\Big),\ 0 \le T_I \le 1,\ 0 \le T_{II} \le 1 \tag{90}$$

where:

$$G_I^m(\mathbf{X}) = \frac{(K_I^m(\mathbf{X}))^2}{E} \tag{91}$$

$$G_{II}^m(\mathbf{X}) = \frac{(K_{II}^m(\mathbf{X}))^2}{E} \tag{92}$$

$$G_I^b(\mathbf{X}) = \frac{\pi}{3}\frac{(K_I^b(\mathbf{X}))^2}{E} \tag{93}$$

$$G_{II}^b(\mathbf{X}) = \frac{\pi}{3}\frac{(K_{II}^b(\mathbf{X}))^2}{E} \tag{94}$$

$$G_{III}^b(\mathbf{X}) = \frac{\pi(1+\nu)}{5}\frac{(K_{III}^b(\mathbf{X}))^2}{E} \tag{95}$$

where T_I and T_{II} are empirically-found coefficients for a particular combination of loads.

The sensitivity of G_{eff} with respect to some geometric variable Z_m is:

$$G_{eff,m}(\mathbf{X}) = G_{I,m}^m(\mathbf{X}) + T_I G_{I,m}^b(\mathbf{X}) + T_{II}\Big(G_{II,m}^m(\mathbf{X}) + G_{II,m}^b(\mathbf{X}) + G_{III,m}^b(\mathbf{X})\Big),\ 0 \le T_I \le 1,\ 0 \le T_{II} \le 1 \tag{96}$$

where:

$$G_{I,m}^m(\mathbf{X}) = \frac{2K_I^m(\mathbf{X})K_{I,m}^m(\mathbf{X})}{E} \tag{97}$$

$$G_{II,m}^m(\mathbf{X}) = \frac{2K_{II}^m(\mathbf{X})K_{II,m}^m(\mathbf{X})}{E} \tag{98}$$

$$G_{I,m}^b(\mathbf{X}) = \frac{\pi}{3}\frac{2K_I^b(\mathbf{X})K_{I,m}^b(\mathbf{X})}{E} \tag{99}$$

$$G_{II,m}^b(\mathbf{X}) = \frac{\pi}{3}\frac{2K_{II}^b(\mathbf{X})K_{II,m}^b(\mathbf{X})}{E} \tag{100}$$

$$G_{III,m}^b(\mathbf{X}) = \frac{\pi(1+\nu)}{5}\frac{2K_{III}^b(\mathbf{X})K_{III,m}^b(\mathbf{X})}{E} \tag{101}$$

Since T_I and T_{II} are unknown, reliability analyses were conducted over a range of combinations of these two coefficients. The results of these analyses can be seen in Figures 8 and 9 which show 3D and 2D representations of the same data respectively. As expected, it can be seen that increasing T_I or T_{II} increases the probability of failure. T_I was shown to have the most influence on the probability of failure, suggesting that mode-I components have more influence than mode-II or mode-III in this example. This is due to the presence of the membrane traction t_2, and the fact that the crack rotation angle is quite low at 30°.

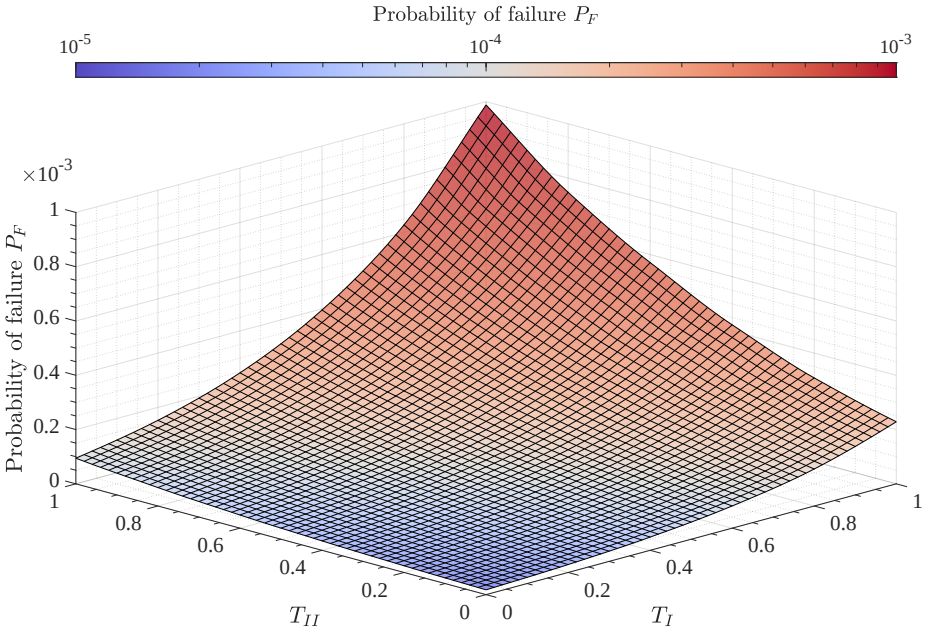

Figure 8: Probabilities of failure P_F evaluated over a range of values for T_I and T_{II} (eqs. 90 and 96). This Figure presents the data as a 3D surface plot.

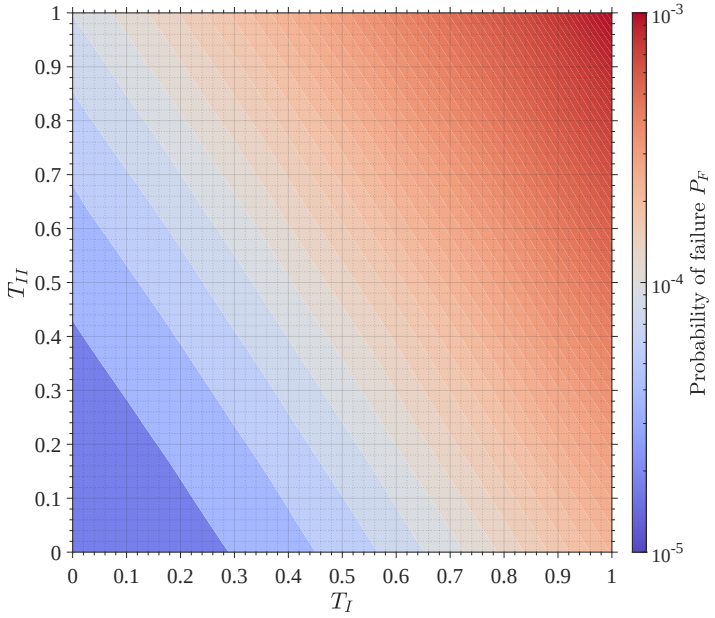

Figure 9: Probabilities of failure P_F evaluated over a range of values for T_I and T_{II} (eqs. 90 and 96). This Figure presents the data as a 2D contour plot.

To compare the levels of influence that the different design variables have on the reliability of the structure, the sensitivities of g with respect to the variables in $\mathbf{Z}$ were calculated and they can be seen in Table 3. It can be seen that among the geometric variables Z_1 to Z_6, that θ and a have the most influence on the reliability of the structure, while variables b_1, b_2, L, and W have much less influence. This is intuitive since θ and a have a much more direct influence on G_{eff}. Negative sensitivities imply that increasing the value of the variable leads reduced reliability. This can be seen with a, t_2, and p_2.

Table 3: Sensitivities of g with respect to the various design variables investigated in this example. The sensitivities are evaluated at the means of each variable. Values of $T_I = 0.5$ and $T_{II} = 0.5$ were used.

Z_i	X_i	Parameter	Normalised sensitivity $\frac{1}{\mu_{G_o}}\frac{\partial g}{\partial \mathrm{X}_i}$ $(\times 10^{-2})$	Units
Z_1	X_1	θ	0.912	rad^{-1}
Z_2	X_2	a	-1.11	m^{-1}
Z_3	X_3	b_1	0.0381	m^{-1}
Z_4	X_4	b_2	0.287	m^{-1}
Z_5	X_5	L	0.159	m^{-1}
Z_6	X_6	W	0.0186	m^{-1}
Z_7	X_7	h	-0.0614	m^{-1}
Z_8	X_8	t_2	-3.42	mN^{-1}
Z_9	X_9	p_2	-1.49	N^{-1}
Z_{10}	X_{10}	q_3	0.339	$\mathrm{m}^2\mathrm{N}^{-1}$
Z_{11}	X_{11}	E	4.54	$\mathrm{m}^2\mathrm{N}^{-1}$
Z_{12}	X_{12}	ν	-0.281	$\mathrm{m}^2\mathrm{J}^{-1}$
Z_{13}	-	G_o	20.0	-

4. Conclusions

In conclusion, a new methodology for determining stress intensity factor (SIF) sensitivities for plate bending problems using the Dual Boundary Element Method (DBEM) has been proposed. A DBEM-based Implicit Differentiation Method (IDM), making use of the direct derivatives of the DBEM integral equations and J-

integral formulations for plate bending - which have been derived for the first time, is used to evaluate SIF sensitivities with respect to geometric parameters such as crack half-length a and crack rotation angle θ. A numerical example featuring a thick plate subjected to membrane, bending, and pressure loads is presented, and the results from the IDM are compared to the relatively crude Finite Difference Method (FDM). It was shown that the IDM and the FDM compared quite well once the optimal step size for the FDM was determined. The SIF sensitivities with respect to crack half-length a showed an average absolute percentage difference between the IDM and the FDM of, at most, 3.07%. The necessary use of a time-consuming optimization procedure to determine the optimal step size for the FDM suggests that the IDM is a significantly more efficient and robust alternative to the FDM for SIF sensitivity evaluation for plate bending problems. In the second half of the numerical example, a demonstration of one possible application of the DBEM-based IDM was presented. This involved carrying out reliability analyses with the plate using the First-Order Reliability Method (FORM) with a large number of design variables.

Appendix A Formulations for DBEM-based IDM

The fundamental solutions for the membrane and for plate bending can be found in [6]. The derivatives of these fundamental solutions with respect to some geometric parameter Z_m have been derived for the first time in this work and are presented in this Appendix.

A.1 Useful Definitions

The following relationships are used in the fundamental solutions derived in this work.

$$r_\alpha = x_\alpha - x'_\alpha \tag{102}$$

$$r = \sqrt{r_\alpha^2} = \sqrt{r_1^2 + r_2^2} \tag{103}$$

$$r_{,\alpha} = \frac{r_\alpha}{r} \tag{104}$$

$$\frac{\partial r}{\partial n} = r_{,n} = n_\alpha r_{,\alpha} = n_1 r_{,1} + n_2 r_{,2} \tag{105}$$

Derivatives with respect to direction x_α:

$$\frac{\partial f(r)}{\partial x_\alpha} = \frac{\partial f(r)}{\partial r}\frac{\partial r}{\partial x_\alpha} = \frac{\partial f(r)}{\partial r} r_{,\alpha} \tag{106}$$

$$r_{,\alpha\beta} = \frac{1}{r}\Big(\delta_{\alpha\beta} - r_{,\alpha} r_{,\beta}\Big) \tag{107}$$

$$(r_{,n})_{,\alpha} = \frac{1}{r}\Big(n_\alpha - r_{,\alpha} r_{,n}\Big) \tag{108}$$

Derivatives with respect to some geometric variable Z_m:

$$\frac{\partial f(r)}{\partial Z_m} = \frac{\partial f(r)}{\partial r}\frac{\partial r}{\partial Z_m} = \frac{\partial f(r)}{\partial r} r_{,m} \tag{109}$$

$$r_{\alpha,m} = x_{\alpha,m} - x'_{\alpha,m} \tag{110}$$

$$r_{,m} = \frac{1}{2}\Big(2r_1 r_{1,m} + 2r_2 r_{2,m}\Big) r^{-1} = r_\alpha r_{\alpha,m} r^{-1} = r_{,\alpha} r_{\alpha,m} \tag{111}$$

$$r_{,\alpha m} = \frac{r_{\alpha,m}}{r} - \frac{r_\alpha}{r^2} r_{,m} = \frac{r_{\alpha,m}}{r} - \frac{r_{,\alpha}}{r} r_{,m} = \frac{1}{r}\Big(r_{\alpha,m} - r_{,\alpha} r_{,m}\Big) \tag{112}$$

$$\left(\frac{\partial r}{\partial n}\right)_{,m} = r_{,nm} = (n_\gamma r_{,\gamma})_{,m} = \left(\frac{1}{r}(n_\gamma r_\gamma)\right)_{,m} = \frac{1}{r}\Big((n_\gamma r_\gamma)_{,m} - r_{,n} r_{,m}\Big) \tag{113}$$

$$(r_{,\alpha} r_{,\beta})_{,m} = \frac{1}{r}\Big(r_{,\alpha} r_{\beta,m} + r_{,\beta} r_{\alpha,m} - 2 r_{,\alpha} r_{,\beta} r_{,m}\Big) \tag{114}$$

$$(n_\gamma r_\gamma)_{,m} = n_{1,m} r_1 + n_{2,m} r_2 + n_1 r_{1,m} + n_2 r_{2,m} \tag{115}$$

Useful definitions for plate bending:

$$\lambda = \sqrt{10}/h \tag{116}$$

$$z = \lambda r \tag{117}$$

$$B = \frac{Eh}{1-\nu^2} \tag{118}$$

$$D = \frac{Eh^3}{12(1-\nu^2)} \tag{119}$$

$$C = \frac{D(1-\nu)\lambda^2}{2} \tag{120}$$

where λ is the shear factor, h is plate thickness, and B, D, and C represent the tension stiffness, bending stiffness, and shear stiffness of the plate respectively.

We also have:

$$A(z) = K_0(z) + \frac{2}{z}\left[K_1(z) - \frac{1}{z}\right] \tag{121}$$

$$B(z) = K_0(z) + \frac{1}{z}\left[K_1(z) - \frac{1}{z}\right] \tag{122}$$

where $K_0(z)$ and $K_1(z)$ are modified Bessel functions of the second kind.

$$A_{,m}(z) = K_{0,m}(z) - \frac{2\lambda r_{,m}}{z^2} K_1(z) + \frac{2}{z} K_{1,m}(z) + \frac{4\lambda r_{,m}}{z^3} \tag{123}$$

$$B_{,m}(z) = K_{0,m}(z) - \frac{\lambda r_{,m}}{z^2} K_1(z) + \frac{1}{z} K_{1,m}(z) + \frac{2\lambda r_{,m}}{z^3} \tag{124}$$

where $K_{0,m}(z)$ and $K_{1,m}(z)$ are:

$$K_{0,m}(z) = -\lambda r_{,m} K_1(z) \tag{125}$$

$$K_{1,m}(z) = -\lambda r_{,m}\left(K_0(z) + \frac{1}{z} K_1(z)\right) \tag{126}$$

$$A_{,\rho}(z) = K_{0,\rho}(z) - \frac{2\lambda r_{,\rho}}{z^2} K_1(z) + \frac{2}{z} K_{1,\rho}(z) + \frac{4\lambda r_{,\rho}}{z^3} \tag{127}$$

$$B_{,\rho}(z) = K_{0,\rho}(z) - \frac{\lambda r_{,\rho}}{z^2} K_1(z) + \frac{1}{z} K_{1,\rho}(z) + \frac{2\lambda r_{,\rho}}{z^3} \tag{128}$$

where $K_{0,\rho}(z)$ and $K_{1,\rho}(z)$ are:

$$K_{0,\rho}(z) = -\lambda r_{,\rho} K_1(z) \tag{129}$$

$$K_{1,\rho}(z) = -\lambda r_{,\rho}\left(K_0(z) + \frac{1}{z} K_1(z)\right) \tag{130}$$

$$A_{,\rho m}(z) = \frac{1}{r^2}\Big(2r_{,\rho}r_{,m} - r_{\rho,m}\Big)\Big(2A(z) + zK_1(z)\Big) - \frac{r_{,\rho}}{r}\Big(2A_{,m}(z) + \lambda r_{,m}K_1(z) + zK_{1,m}(z)\Big) \tag{131}$$

$$B_{,\rho m}(z) = \frac{1}{r^2}\Big(2r_{,\rho}r_{,m} - r_{\rho,m}\Big)\Big(A(z) + zK_1(z)\Big) - \frac{r_{,\rho}}{r}\Big(A_{,m}(z) + \lambda r_{,m}K_1(z) + zK_{1,m}(z)\Big) \tag{132}$$

where $K_{0,\rho m}(z)$ and $K_{1,\rho m}(z)$ are:

$$K_{0,\rho m}(z) = -\lambda\Big(r_{,\rho m}K_1(z) + r_{,\rho}K_{1,m}(z)\Big) \tag{133}$$

$$K_{1,\rho m}(z) = -\lambda\left[r_{,\rho m}K_0(z) + r_{,\rho}K_{0,m}(z) - \frac{\lambda r_{,\rho}r_{,m}}{z^2}K_1(z) + \frac{1}{z}\Big(r_{,\rho m}K_1(z) + r_{,\rho}K_{1,m}(z)\Big)\right] \tag{134}$$

A.2 Membrane

The derivatives of the membrane fundamental solutions are:

$$U_{\alpha\beta,m} = \frac{1+\nu}{4\pi Eh(1-\nu)r}\Big[r_{\alpha,m}r_{,\beta} + r_{,\alpha}r_{\beta,m} - ((3-4\nu)\delta_{\alpha\beta} + 2r_{,\alpha}r_{,\beta})r_{,m}\Big] \tag{135}$$

$$\begin{aligned} U_{\alpha\beta,\rho m} = &-\frac{r_{,m}}{r}U_{\alpha\beta,\rho} + \frac{1+\nu}{4\pi Eh(1-\nu)r}\Big[(3-4\nu)\delta_{\alpha\beta}r_{,\rho m} - \delta_{\beta\rho}r_{,\alpha m} - \delta_{\alpha\rho}r_{,\beta m} \\ &+ 2r_{,\rho}(r_{,\alpha m}r_{,\beta} + r_{,\alpha}r_{,\beta m}) + 2r_{,\alpha}r_{,\beta}r_{,\rho m}\Big] \end{aligned} \tag{136}$$

$$\begin{aligned} T_{\alpha\beta,m} = &-\frac{1}{4\pi(1-\nu)r^2}\Big[2r_{,n}(r_{\alpha,m}r_{,\beta} + r_{,\alpha}r_{\beta,m} - ((1-2\nu)\delta_{\alpha\beta} + 4r_{,\alpha}r_{,\beta})r_{,m}) \\ &+ (n_\gamma r_\gamma)_{,m}((1-2\nu)\delta_{\alpha\beta} + 2r_{,\alpha}r_{,\beta}) + (1-2\nu)(n_{\alpha,m}r_\beta - n_{\beta,m}r_\alpha \\ &+ n_\alpha r_{\beta,m} - n_\beta r_{\alpha,m}) - 2(1-2\nu)(n_\alpha r_{,\beta} - n_\beta r_{,\alpha})r_{,m}\Big] \end{aligned} \tag{137}$$

$$\begin{aligned} T_{\alpha\beta,\rho m} = &-\frac{2r_{,m}}{r}T_{\alpha\beta,\rho} + \frac{1}{4\pi(1-\nu)r^2}\left[2r_{,nm}\Big(\delta_{\alpha\rho}r_{,\beta} + \delta_{\beta\rho}r_{,\alpha} - r_{,\rho}\Big((1-2\nu)\delta_{\alpha\beta} + 4r_{,\alpha}r_{,\beta}\Big)\Big)\right. \\ &+ 2r_{,n}\Big(\delta_{\alpha\rho}r_{,\beta m} + \delta_{\beta\rho}r_{,\alpha m} - r_{,\rho m}\Big((1-2\nu)\delta_{\alpha\beta} + 4r_{,\alpha}r_{,\beta}\Big) - 4r_{,\rho}\Big(r_{,\alpha m}r_{,\beta} + r_{,\alpha}r_{,\beta m}\Big)\Big) \\ &+ n_{\rho,m}\Big((1-2\nu)\delta_{\alpha\beta} + 2r_{,\alpha}r_{,\beta}\Big) + 2n_\rho\Big(r_{,\alpha m}r_{,\beta} + r_{,\alpha}r_{,\beta m}\Big) \\ &- n_{\beta,m}(1-2\nu)\Big(\delta_{\alpha\rho} - 2r_{,\alpha}r_{,\rho}\Big) + 2n_\beta(1-2\nu)\Big(r_{,\alpha m}r_{,\rho} + r_{,\alpha}r_{,\rho m}\Big) \\ &\left.+ n_{\alpha,m}(1-2\nu)\Big(\delta_{\beta\rho} - 2r_{,\beta}r_{,\rho}\Big) - 2n_\alpha(1-2\nu)\Big(r_{,\beta m}r_{,\rho} + r_{,\beta}r_{,\rho m}\Big)\right] \end{aligned} \tag{138}$$

$$\begin{aligned} D_{\rho\alpha\beta,m} = &-\frac{r_{,m}}{r}D_{\rho\alpha\beta} + \frac{1}{4\pi(1-\nu)r}\Big[2r_{,\rho}(r_{,\alpha m}r_{,\beta} + r_{,\alpha}r_{,\beta m}) + 2r_{,\alpha}r_{,\beta}r_{,\rho m} \\ &+ (1-2\nu)(-\delta_{\alpha\beta}r_{,\rho m} + \delta_{\rho\alpha}r_{,\beta m} + \delta_{\beta\rho}r_{,\alpha m})\Big] \end{aligned} \tag{139}$$

$$S_{\rho\alpha\beta,m} = -\frac{2r_{,m}}{r}S_{\rho\alpha\beta} + \frac{Eh}{4\pi(1-\nu^2)r^2}\Bigg[2r_{,nm}\Big((1-2\nu)\delta_{\alpha\beta}r_{,\rho} + \nu(\delta_{\alpha\rho}r_{,\beta} + \delta_{\beta\rho}r_{,\alpha}) - 4r_{,\alpha}r_{,\beta}r_{,\rho}\Big) \tag{140}$$

$$+ 2r_{,n}\Big((1-2\nu)\delta_{\alpha\beta}r_{,\rho m} + \nu(\delta_{\alpha\rho}r_{,\beta m} + \delta_{\beta\rho}r_{,\alpha m}) - 4r_{,\rho}(r_{,\alpha m}r_{,\beta} + r_{,\alpha}r_{,\beta m}) - 4r_{,\alpha}r_{,\beta}r_{,\rho m}\Big)$$

$$+ 2\nu(n_{\alpha,m}r_{,\beta}r_{,\rho} + n_{\alpha}(r_{,\beta m}r_{,\rho} + r_{,\beta}r_{,\rho m}) + n_{\beta,m}r_{,\alpha}r_{,\rho} + n_{\beta}(r_{,\alpha m}r_{,\rho} + r_{,\alpha}r_{,\rho m}))$$

$$+ (1-2\nu)(2n_{\rho,m}r_{,\alpha}r_{,\beta} + 2n_{\rho}(r_{,\alpha m}r_{,\beta} + r_{,\alpha}r_{,\beta m}) + \delta_{\alpha\rho}n_{\beta,m} + \delta_{\beta\rho}n_{\alpha,m}) - (1-4\nu)\delta_{\alpha\beta}n_{\rho,m}\Bigg]$$

A.3 Plate Bending

The derivatives of the plate bending fundamental solutions are:

For $U^b_{ij,m}$:

$$U^b_{\alpha\beta,m} = \frac{1}{8\pi D(1-\nu)r}\Bigg\{\Big[8rB_{,m}(z) + 2(\nu-1)r_{,m}\Big]\delta_{\alpha\beta} - 8rA_{,m}(z)r_{,\alpha}r_{,\beta} \tag{141}$$

$$- \Big[8A(z) + 2(1-\nu)\Big]\Big(r_{,\alpha}r_{\beta,m} + r_{,\beta}r_{\alpha,m} - 2r_{,\alpha}r_{,\beta}r_{,m}\Big)\Bigg\}$$

$$U^b_{\alpha 3,m} = \frac{1}{8\pi D}\Big[2r_{,m}r_{,\alpha} + (2\ln z - 1)r_{\alpha,m}\Big] \tag{142}$$

$$U^b_{3\alpha,m} = U^b_{\alpha 3,m} \tag{143}$$

$$U^b_{33,m} = \frac{1}{8\pi D(1-\nu)\lambda^2 r}\Big[(1-\nu)(2\ln z - 1)z^2 - 8\Big]r_{,m} \tag{144}$$

For $U^b_{ij,\rho m}$:

$$U^b_{\alpha\beta,\rho m} = -\frac{r_{,m}}{r}U^b_{\alpha\beta,\rho} - \frac{1}{8\pi D(1-\nu)r}\Bigg[\Big(8B_{,\rho m}(z)r + 8B_{,\rho}(z)r_{,m} - 2(1-\nu)r_{,\rho m}\Big)\delta_{\alpha\beta} \tag{145}$$

$$- 8A_{,\rho m}rr_{,\alpha}r_{,\beta} - 8A_{,\rho}(z)\Big(r_{,\alpha}r_{\beta,m} + r_{\alpha,m}r_{,\beta} - 2r_{,\alpha}r_{,\beta}r_{,m}\Big)$$

$$- 8A_{,m}(z)\Big(\delta_{\alpha\rho}r_{,\beta} + \delta_{\beta\rho}r_{,\alpha} - 2r_{,\alpha}r_{,\beta}r_{,\rho}\Big)$$

$$- \Big(8A(z) + 2(1-\nu)\Big)\Big(\delta_{\alpha\rho}r_{,\beta m} + \delta_{\beta\rho}r_{,\alpha m} - 2r_{,\alpha}r_{,\beta}r_{,\rho m} - 2r_{,\rho}(r_{,\alpha m}r_{,\beta} + r_{,\alpha}r_{,\beta m})\Big)\Bigg]$$

$$U^b_{\alpha 3,\rho m} = -\frac{1}{4\pi Dr}\Big[r_{\alpha,m}r_{,\rho} + r_{\rho,m}r_{,\alpha} - 2r_{,\alpha}r_{,\rho}r_{,m} + r_{,m}\delta_{\alpha\rho}\Big] \tag{146}$$

$$U^b_{3\alpha,\rho m} = -U^b_{\alpha 3,\rho m} \tag{147}$$

$$U^b_{33,\rho m} = -\frac{1}{8\pi D(1-\nu)\lambda^2 r^2}\Bigg[(r_{\rho,m}-2r_{,\rho}r_{,m})\Big((1-\nu)z^2(2\ln z-1)-8\Big)+4(1-\nu)r_{,\rho}r_{,m}z^2\ln z\Bigg] \tag{148}$$

For $T^b_{ij,m}$:

$$\begin{aligned}
T^b_{\alpha\beta,m} &= -\frac{r_{,m}}{r}T^b_{\alpha\beta} - \frac{1}{4\pi r}\Bigg[\Big(4A_{,m}(z)+2\lambda r_{,m}K_1(z)+2zK_{1,m}(z)\Big)\Big(\delta_{\alpha\beta}r_{,n}+r_{,\beta}n_\alpha\Big) \\
&+\Big(4A(z)+2zK_1(z)+1-\nu\Big)\Big(\delta_{\alpha\beta}r_{,nm}+r_{,\beta m}n_\alpha+r_{,\beta}n_{\alpha,m}\Big) \\
&+4A_{,m}(z)r_{,\alpha}n_\beta+\Big(4A(z)+1+\nu\Big)\Big(r_{,\alpha m}n_\beta+r_{,\alpha}n_{\beta,m}\Big) \\
&-2\Big(8A_{,m}(z)+2\lambda r_{,m}K_1(z)+2zK_{1,m}(z)\Big)r_{,\alpha}r_{,\beta}r_{,n} \\
&-2\Big(8A(z)+2zK_1(z)+1-\nu\Big)\Big(r_{,\alpha}r_{,\beta}r_{,nm}+\big(r_{,\alpha m}r_{,\beta}+r_{,\alpha}r_{,\beta m}\big)r_{,n}\Big)\Bigg]
\end{aligned} \tag{149}$$

$$T^b_{\alpha 3,m} = \frac{\lambda^2}{2\pi}\Big[B_{,m}(z)n_\alpha + B(z)n_{\alpha,m} - A_{,m}(z)r_{,\alpha}r_{,n} - A(z)\big(r_{,\alpha m}r_{,n}+r_{,\alpha}r_{,nm}\big)\Big] \tag{150}$$

$$T^b_{3\alpha,m} = -\frac{(1-\nu)}{8\pi}\Bigg[2\frac{(1+\nu)}{(1-\nu)}\Big(\frac{r_{,m}}{r}n_\alpha + n_{\alpha,m}\ln z\Big) - n_{\alpha,m} + 2\Big(r_{,\alpha m}r_{,n}+r_{,\alpha}r_{,nm}\Big)\Bigg] \tag{151}$$

$$T^b_{33,m} = -\frac{1}{2\pi r^2}\Big[(n_\gamma r_\gamma)_{,m} - 2r_{,n}r_{,m}\Big] \tag{152}$$

For $T^b_{ij,\rho m}$:

$$\begin{aligned}
T^b_{\alpha\beta,\rho m} &= \frac{r_{\rho,m}}{r^2}T^b_{\alpha\beta} + \frac{r_{,\rho}}{r}T^b_{\alpha\beta,m} - \frac{2r_{,m}}{r}T^b_{\alpha\beta,\rho} \\
&+\frac{1}{4\pi r^2}\Bigg[2\Big(2A_{,\rho m}(z)+\lambda r_{,\rho m}K_1(z)+\lambda r_{,\rho}K_{1,m}(z)+\lambda r_{,m}K_{1,\rho}(z)+zK_{1,\rho m}(z)\Big)\Big(\delta_{\alpha\beta}(n_\gamma r_\gamma)+r_\beta n_\alpha\Big) \\
&+2\Big(2A_{,\rho}(z)+\lambda r_{,\rho}K_1(z)+zK_{1,\rho}(z)\Big)\Big(\delta_{\alpha\beta}(n_\gamma r_\gamma)_{,m}+r_\beta n_{\alpha,m}+r_{\beta,m}n_\alpha\Big) \\
&+2\Big(2A_{,m}(z)+\lambda r_{,m}K_1(z)+zK_{1,m}(z)\Big)\Big(\delta_{\alpha\beta}(n_\rho-r_{,\rho}r_{,n})+n_\alpha(\delta_{\beta\rho}-r_{,\beta}r_{,\rho})\Big) \\
&+\Big(4A(z)+2zK_1(z)+1-\nu\Big) \\
&\times\Big(\delta_{\alpha\beta}(n_{\rho,m}-r_{,\rho m}r_{,n}-r_{,\rho}r_{,nm})+n_{\alpha,m}(\delta_{\beta\rho}-r_{,\beta}r_{,\rho})-n_\alpha(r_{,\beta m}r_{,\rho}+r_{,\beta}r_{,\rho m})\Big) \\
&+4A_{,\rho m}(z)r_\alpha n_\beta + 4A_{,\rho}(z)(r_{\alpha,m}n_\beta + r_\alpha n_{\beta,m}) \\
&+4A_{,m}(z)\Big(\delta_{\alpha\rho}-r_{,\alpha}r_{,\rho}\Big)n_\beta + \Big(4A(z)+1+\nu\Big)\Big(\delta_{\alpha\rho}n_{\beta,m}-r_{,\alpha}r_{,\rho}n_{\beta,m}-n_\beta(r_{,\alpha m}r_{,\rho}+r_{,\alpha}r_{,\rho m})\Big) \\
&-4\Big(4A_{,\rho m}(z)+\lambda r_{,\rho m}K_1(z)+\lambda r_{,\rho}K_{1,m}(z)+\lambda r_{,m}K_{1,\rho}(z)+zK_{1,\rho m}(z)\Big)r_{,\alpha}r_{,\beta}(n_\gamma r_\gamma) \\
&-4\Big(4A_{,\rho}(z)+\lambda r_{,\rho}K_1(z)+zK_{1,\rho}(z)\Big)\Big(r_{,\alpha}r_{,\beta}(n_\gamma r_\gamma)_{,m}+(n_\gamma r_\gamma)(r_{,\alpha m}r_{,\beta}+r_{,\alpha}r_{,\beta m})\Big) \\
&-4\Big(4A_{,m}(z)+\lambda r_{,m}K_1(z)+zK_{1,m}(z)\Big)\Big(r_{,\alpha}r_{,\beta}n_\rho+r_{,n}(\delta_{\alpha\rho}r_{,\beta}+\delta_{\beta\rho}r_{,\alpha}-3r_{,\alpha}r_{,\beta}r_{,\rho})\Big) \\
&-2\Big(8A(z)+2zK_1(z)+1-\nu\Big) \\
&\times\Big(r_{,\alpha}r_{,\beta}n_{\rho,m}+n_\rho(r_{,\alpha m}r_{,\beta}+r_{,\alpha}r_{,\beta m})+r_{,nm}(\delta_{\alpha\rho}r_{,\beta}+\delta_{\beta\rho}r_{,\alpha}-3r_{,\alpha}r_{,\beta}r_{,\rho}) \\
&+r_{,n}\big(\delta_{\alpha\rho}r_{,\beta m}+\delta_{\beta\rho}r_{,\alpha m}-3r_{,\alpha}r_{,\beta}r_{,\rho m}-3r_{,\rho}(r_{,\alpha m}r_{,\beta}+r_{,\alpha}r_{,\beta m})\big)\Big)\Bigg]
\end{aligned} \tag{153}$$

$$T^b_{\alpha 3,\rho m} = -\frac{r_{,m}}{r}T^b_{\alpha 3,\rho} - \frac{\lambda^2}{2\pi r}\Bigg[B_{,\rho m}(z) r n_\alpha + B_{,\rho}(z)\Big(r_{,m}n_\alpha + r n_{\alpha,m}\Big) \tag{154}$$
$$- A_{,\rho m}(z) r_\alpha r_{,n} - A_{,\rho}(z)\Big(r_{\alpha,m}r_{,n} + r_\alpha r_{,nm}\Big)$$
$$- A_{,m}(z)\Big(\delta_{\alpha\rho}r_{,n} + r_{,\alpha}n_\rho - 2r_{,\alpha}r_{,\rho}r_{,n}\Big)$$
$$- A(z)\Big(\delta_{\alpha\rho}r_{,nm} + r_{,\alpha m}n_\rho + r_{,\alpha}n_{\rho,m} - 2r_{,\alpha}r_{,\rho}r_{,nm} - 2r_{,n}(r_{,\alpha m}r_{,\rho} + r_{,\alpha}r_{,\rho m})\Big)\Bigg]$$

$$T^b_{3\alpha,\rho m} = -\frac{r_{,m}}{r}T^b_{3\alpha,\rho} + \frac{(1-\nu)}{8\pi r}\Bigg[2\frac{(1+\nu)}{(1-\nu)}\Big(r_{,\rho m}n_\alpha + r_{,\rho}n_{\alpha,m}\Big) \tag{155}$$
$$+ 2\Big(r_{,\alpha m}n_\rho + r_{,\alpha}n_{\rho,m} + r_{,nm}(\delta_{\alpha\rho} - 2r_{,\alpha}r_{,\rho}) - 2r_{,n}(r_{,\alpha m}r_{,\rho} + r_{,\alpha}r_{,\rho m})\Big)\Bigg]$$

$$T^b_{33,\rho m} = -\frac{2r_{,m}}{r}T^b_{33,\rho} + \frac{1}{2\pi r^2}\Bigg[n_{\rho,m} - 2\Big(r_{,\rho m}r_{,n} + r_{,\rho}r_{,nm}\Big)\Bigg] \tag{156}$$

For $V^b_{i,\beta m}$:

$$V^b_{\alpha,\beta m} = \frac{2}{r}r_{,m}V^b_{\alpha,\beta} + \frac{r}{128\pi D}\Big[4r_{,m}\big(\delta_{\alpha\beta} + 2r_{,\alpha}r_{,\beta}\big) + 2\big(4\ln z - 3\big)\big(r_{,\alpha}r_{\beta,m} + r_{,\beta}r_{\alpha,m} - 2r_{,\alpha}r_{,\beta}r_{,m}\big)\Big] \tag{157}$$

$$V^b_{3,\beta m} = -\frac{1}{128\pi D(1-\nu)\lambda^2}\Bigg\{r_{\beta,m}\Big[32\big(2\ln z - 1\big) - z^2(1-\nu)(4\ln z - 5)\Big] \tag{158}$$
$$+ 2r_{,\beta}r_{,m}\Big[32 - z^2(1-\nu)(4\ln z - 3)\Big]\Bigg\}$$

For $V^b_{i,\beta\rho m}$:

$$V^b_{\alpha,\beta\rho m} = \frac{r_{,m}}{r}V^b_{\alpha,\beta\rho} - \frac{r}{64\pi D}\Bigg[4\frac{r_{,m}}{r}\Big(\delta_{\alpha\beta}r_{,\rho} + \delta_{\alpha\rho}r_{,\beta} + \delta_{\beta\rho}r_{,\alpha}\Big) \tag{159}$$
$$+ \Big(4\ln z - 3\Big)\Big(\delta_{\alpha\beta}r_{,\rho m} + \delta_{\alpha\rho}r_{,\beta m} + \delta_{\beta\rho}r_{,\alpha m}\Big) + 4r_{,\alpha}r_{,\beta}r_{,\rho m} + 4r_{,\rho}\Big(r_{,\alpha}r_{,\beta m} + r_{,\beta}r_{,\alpha m}\Big)\Bigg]$$

$$V^b_{3,\beta\rho m} = \frac{1}{64\pi D(1-\nu)\lambda^2 r}\Bigg[\Big(\delta_{\beta\rho}r_{,m} + r_{,\beta}r_{\rho,m} + r_{,\rho}r_{\beta,m}\Big)\Big(32 - (1-\nu)z^2(4\ln z - 3)\Big) \tag{160}$$
$$- 4r_{,\beta}r_{,\rho}r_{,m}\Big(16 + (1-\nu)z^2\Big)\Bigg]$$

For $D^b_{i\beta k,m}$:

$$D^b_{\alpha\beta\rho,m} = -\frac{r_{,m}}{r}D^b_{\alpha\beta\rho} + \frac{1}{4\pi r}\Big[\Big(4A_{,m}(z) + 2\lambda r_{,m}K_1(z) + 2zK_{1,m}\Big)\Big(\delta_{\beta\rho}r_{,\alpha} + \delta_{\alpha\rho}r_{,\beta}\Big) \tag{161}$$
$$+ \Big(4A(z) + 2zK_1(z) + 1 - \nu\Big)\Big(\delta_{\beta\rho}r_{,\alpha m} + \delta_{\alpha\rho}r_{,\beta m}\Big)$$
$$- 2\Big(8A_{,m}(z) + 2\lambda r_{,m}K_1(z) + 2zK_{1,m}\Big)r_{,\alpha}r_{,\beta}r_{,\rho}$$
$$- 2\Big(8A(z) + 2zK_1(z) + 1 - \nu\Big)\Big(r_{,\rho}\big(r_{,\alpha m}r_{,\beta} + r_{,\alpha}r_{,\beta m}\big) + r_{,\rho m}r_{,\alpha}r_{,\beta}\Big)$$
$$+ 4A_{,m}(z)\delta_{\alpha\beta}r_{,\rho} + \Big(4A(z) + 1 + \nu\Big)\delta_{\alpha\beta}r_{,\rho m}\Big]$$

$$D^b_{\alpha\beta 3,m} = -\frac{(1-\nu)}{8\pi r}\Big[2\big(r_{,\alpha}r_{\beta,m} + r_{,\beta}r_{\alpha,m}\big) - r_{,m}\Big(4r_{,\alpha}r_{,\beta} - 2\frac{(1+\nu)}{(1-\nu)}\delta_{\alpha\beta}\Big)\Big] \tag{162}$$

$$D^b_{3\beta\rho,m} = \frac{\lambda^2}{2\pi}\Big[B_{,m}(z)\delta_{\rho\beta} - A_{,m}(z)r_{,\rho}r_{,\beta} - A(z)\big(r_{,\rho m}r_{,\beta} + r_{,\rho}r_{,\beta m}\big)\Big] \tag{163}$$

$$D^b_{3\beta 3,m} = \frac{1}{2\pi r^2}\big(r_{\beta,m} - 2r_{,\beta}r_{,m}\big) \tag{164}$$

For $S^b_{i\beta k,m}$:

$$S^b_{\alpha\beta\rho,m} = -\frac{2r_{,m}}{r}S^b_{\alpha\beta\rho} + \frac{D(1-\nu)}{4\pi r^2}\Big[\Big(4A_{,m}(z) + 2\lambda r_{,m}K_1(z) + 2zK_{1,m}(z)\Big)\Big(\delta_{\rho\alpha}n_\beta + \delta_{\rho\beta}n_\alpha\Big) \tag{165}$$
$$+ \Big(4A(z) + 2zK_1(z) + 1 - \nu\Big)\Big(\delta_{\rho\alpha}n_{\beta,m} + \delta_{\rho\beta}n_{\alpha,m}\Big) + 4A_{,m}(z)\delta_{\alpha\beta}n_\rho + \Big(4A(z) + 1 + 3\nu\Big)\delta_{\alpha\beta}n_{\rho,m}$$
$$- \Big(16A_{,m}(z) + 6\lambda r_{,m}K_1(z) + 6zK_{1,m}(z) + 2z\lambda r_{,m}K_0(z) + z^2K_{0,m}(z)\Big)$$
$$\times \Big((n_\alpha r_{,\beta} + n_\beta r_{,\alpha})r_{,\rho} + (\delta_{\rho\alpha}r_{,\beta} + \delta_{\rho\beta}r_{,\alpha})r_{,n}\Big)$$
$$- \Big(16A(z) + 6zK_1(z) + z^2K_0(z) + 2 - 2\nu\Big)\Big((n_{\alpha,m}r_{,\beta} + n_\alpha r_{,\beta m} + n_{\beta,m}r_{,\alpha} + n_\beta r_{,\alpha m})r_{,\rho}$$
$$+ (n_\alpha r_{,\beta} + n_\beta r_{,\alpha})r_{,\rho m} + (\delta_{\rho\alpha}r_{,\beta m} + \delta_{\rho\beta}r_{,\alpha m})r_{,n} + (\delta_{\rho\alpha}r_{,\beta} + \delta_{\rho\beta}r_{,\alpha})r_{,nm}\Big)$$
$$- 2\Big(8A_{,m}(z) + 2\lambda r_{,m}K_1(z) + 2zK_{1,m}(z)\Big)\Big(\delta_{\alpha\beta}r_{,\rho}r_{,n} + n_\rho r_{,\alpha}r_{,\beta}\Big)$$
$$- 2\Big(8A(z) + 2zK_1(z) + 1 + \nu\Big)\Big(\delta_{\alpha\beta}(r_{,\rho m}r_{,n} + r_{,\rho}r_{,nm}) + n_\rho(r_{,\alpha m}r_{,\beta} + r_{,\alpha}r_{,\beta m}) + n_{\rho,m}r_{,\alpha}r_{,\beta}\Big)$$
$$+ 4r_{,\alpha}r_{,\beta}r_{,\rho}r_{,n}\Big(24A_{,m}(z) + 8\lambda r_{,m}K_1(z) + 8zK_{1,m}(z) + 2z\lambda r_{,m}K_0(z) + z^2K_{0,m}(z)\Big)$$
$$+ 4\Big(24A(z) + 8zK_1(z) + z^2K_0(z) + 2 - 2\nu\Big)$$
$$\times \Big(r_{,\rho}r_{,n}(r_{,\alpha m}r_{,\beta} + r_{,\alpha}r_{,\beta m}) + r_{,\alpha}r_{,\beta}(r_{,\rho m}r_{,n} + r_{,\rho}r_{,nm})\Big)\Big]$$

$$S^b_{\alpha\beta 3,m} = -\frac{r_{,m}}{r}S^b_{\alpha\beta 3} + \frac{D(1-\nu)\lambda^2}{4\pi r}\Big[\Big(2A_{,m}(z) + \lambda r_{,m}K_1(z) + zK_{1,m}(z)\Big)\Big(r_{,\beta}n_\alpha + r_{,\alpha}n_\beta\Big) \tag{166}$$
$$+ \Big(2A(z) + zK_1(z)\Big)\Big(r_{,\beta m}n_\alpha + r_{,\beta}n_{\alpha,m} + r_{,\alpha m}n_\beta + r_{,\alpha}n_{\beta,m}\Big)$$
$$- 2\Big(4A_{,m}(z) + \lambda r_{,m}K_1(z) + zK_{1,m}\Big)r_{,\alpha}r_{,\beta}r_{,n}$$
$$- 2\Big(4A(z) + zK_1(z)\Big)\Big(r_{,n}(r_{,\alpha m}r_{,\beta} + r_{,\alpha}r_{,\beta m}) + r_{,\alpha}r_{,\beta}r_{,nm}\Big)$$
$$+ 2A_{,m}(z)\delta_{\alpha\beta}r_{,n} + 2A(z)\delta_{\alpha\beta}r_{,nm}\Big]$$

$$S^b_{3\beta\rho,m} = -\frac{r_{,m}}{r}S^b_{3\beta\rho} - \frac{D(1-\nu)\lambda^2}{4\pi r}\Bigg[\Big(2A_{,m}(z) + \lambda r_{,m}K_1(z) + zK_{1,m}(z)\Big)\Big(\delta_{\rho\beta}r_{,n} + r_{,\rho}n_\beta\Big) \tag{167}$$
$$+ \Big(2A(z) + zK_1(z)\Big)\Big(\delta_{\rho\beta}r_{,nm} + r_{,\rho m}n_\beta + r_{,\rho}n_{\beta,m}\Big)$$
$$- 2\Big(4A_{,m}(z) + \lambda r_{,m}K_1(z) + zK_{1,m}(z)\Big)r_{,\rho}r_{,\beta}r_{,n}$$
$$- 2\Big(4A(z) + zK_1(z)\Big)\Big(r_{,n}(r_{,\rho m}r_{,\beta} + r_{,\rho}r_{,\beta m}) + r_{,\rho}r_{,\beta}r_{,nm}\Big)$$
$$+ 2A_{,m}(z)n_\rho r_{,\beta} + 2A(z)\Big(n_{\rho,m}r_{,\beta} + n_\rho r_{,\beta m}\Big)\Bigg]$$

$$S^b_{3\beta 3,m} = -\frac{2r_{,m}}{r}S^b_{3\beta 3} + \frac{D(1-\nu)\lambda^2}{4\pi r^2}\Bigg[n_\beta\Big(2z\lambda r_{,m}B(z) + z^2B_{,m}(z)\Big) + n_{\beta,m}\Big(z^2B(z) + 1\Big) \tag{168}$$
$$- r_{,\beta}r_{,n}\Big(2z\lambda r_{,m}A(z) + z^2A_{,m}(z)\Big) - \Big(z^2A(z) + 2\Big)\Big(r_{,\beta m}r_{,n} + r_{,\beta}r_{,nm}\Big)\Bigg]$$

For $Q^*_{i\beta,m}$:

$$Q^*_{\alpha\beta,m} = \frac{r_{,m}}{r}Q^*_{\alpha\beta} - \frac{r}{64\pi}\Bigg[4\frac{r_{,m}}{r}\Big((1-\nu)(r_{,\beta}n_\alpha + r_{,\alpha}n_\beta) + (1+3\nu)\delta_{\alpha\beta}r_{,n}\Big) \tag{169}$$
$$+ \Big(4\ln z - 3\Big)\Big((1-\nu)(r_{,\beta m}n_\alpha + r_{,\beta}n_{\alpha,m} + r_{,\alpha m}n_\beta + r_{,\alpha}n_{\beta,m}) + (1+3\nu)\delta_{\alpha\beta}r_{,nm}\Big)$$
$$+ 4r_{,nm}\Big((1-\nu)r_{,\alpha}r_{,\beta} + \nu\delta_{\alpha\beta}\Big) + 4(1-\nu)r_{,n}(r_{,\alpha m}r_{,\beta} + r_{,\alpha}r_{,\beta m})\Bigg]$$

$$Q^*_{3\beta,m} = \frac{1}{8\pi}\Bigg[2\frac{r_{,m}}{r}n_\beta + \Big(2\ln z - 1\Big)n_{\beta,m} + 2\Big(r_{,\beta m}r_{,n} + r_{,\beta}r_{,nm}\Big)\Bigg] \tag{170}$$

A.4 Discretisation

When discretising the integral equations seen in sections 2.1-2.4, a transformation has to be made from global coordinates (x_i) to the local coordinates (η) of the elements that make up this discretisation. This transformation is accomplished by calculating the Jacobian of each element n_e and is described in detail in [6]. The derivatives of the Jacobian of some element n_e with respect to some geometric variable Z_m is:

$$J^{n_e}_{,m}(\eta) = \frac{1}{J^{n_e}(\eta)}\left[\frac{d\mathrm{x}^{n_e}_1(\eta)}{d\eta}\frac{d\mathrm{x}^{n_e}_{1,m}(\eta)}{d\eta} + \frac{d\mathrm{x}^{n_e}_2(\eta)}{d\eta}\frac{d\mathrm{x}^{n_e}_{2,m}(\eta)}{d\eta}\right] \tag{171}$$

where:

$$\mathrm{x}^{n_e}_{\alpha,m}(\eta) = \sum_{k=1}^{M} N^{n_e k}(\eta)x^{n_e k}_{\alpha,m} \tag{172}$$

$$\left(\frac{d\mathrm{x}^{n_e}_\alpha(\eta)}{d\eta}\right)_{,m} = \frac{d\mathrm{x}^{n_e}_{\alpha,m}(\eta)}{d\eta} = \sum_{k=1}^{M}\frac{dN^{n_e k}(\eta)}{d\eta}x^{n_e k}_{\alpha,m} \tag{173}$$

k denotes the local node number, and M is the total number of nodes present in each element (for quadratic elements $M = 3$). Quadratic elements are used in this work. Therefore k can equal 1, 2, or 3.
The derivatives of the outward unit normals of some element n_e can also be calculated:

$$n_{1,m}^{n_e}(\eta) = \frac{1}{J^{n_e}(\eta)} \left[\frac{dx_{2,m}^{n_e}(\eta)}{d\eta} - n_1^{n_e}(\eta) J_{,m}^{n_e}(\eta) \right] \tag{174}$$

$$n_{2,m}^{n_e}(\eta) = -\frac{1}{J^{n_e}(\eta)} \left[\frac{dx_{1,m}^{n_e}(\eta)}{d\eta} + n_2^{n_e}(\eta) J_{,m}^{n_e}(\eta) \right] \tag{175}$$

References

References

[1] D. P. Rooke and D. J. Cartwright. *Compendium of Stress Intensity Factors*. MOD, 1976.

[2] D. P. Rooke, D. B. Rayaprolu, and M. H. Aliabadi. Crackline and edge green's functions for stress intensity factors of inclined edge cracks. *Fatigue and Fracture of Engineering Materials and Structures*, 15(5):441–461, 1992.

[3] D. P. Rooke. An improved compounding method for calculating stress-intensity factors. *Engineering Fracture Mechanics*, 23(5):783–792, 1986.

[4] M. H. Aliabadi, D. P. Rooke, and D. J. Cartwright. Mixed-mode bueckner weight functions using boundary element analysis. *International Journal of Fracture*, 34(2):131–147, 1987.

[5] A. Haldar and S. Mahadevan. *Probability, Reliability and Statistical Methods in Engineering Design*. John Wiley and Sons, 1999.

[6] M. H. Aliabadi. *The Boundary Element Method: Applications in solids and structures*, volume 2. John Wiley and Sons, 2002.

[7] T. Dirgantara and M. H. Aliabadi. Crack growth analysis of plates loaded by bending and tension using dual boundary element method. *International Journal of Fracture*, 105(1):27–47, 1999.

[8] A. T. Zehnder and M. J. Viz. Fracture mechanics of thin plates and shells under combined membrane, bending, and twisting loads. *Applied Mechanics Reviews*, 58(1):37–48, 2005. doi: 10.1115/1.1828049.

[9] C. Di Pisa, M. H. Aliabadi, and A. Young. Dual boundary method for assembled plate structures undergoing large deflection. *International Journal for Numerical Methods in Engineering*, 89(13):1720–1738, 2012. ISSN 00295981. doi: 10.1002/nme.3310.

[10] J. Li, Z. Sharif Khodaei, and M. H. Aliabadi. Dynamic dual boundary element analyses for cracked mindlin plates. *International Journal of Solids and Structures*, 152-153:248–260, 2018. ISSN 00207683. doi: 10.1016/j.ijsolstr.2018.06.033.

[11] C. Di Pisa and M. H. Aliabadi. Fatigue crack growth analysis of assembled plate structures with dual boundary element method. *Engineering Fracture Mechanics*, 98:200–213, 2013. ISSN 00137944. doi: 10.1016/j.engfracmech.2012.09.032.

[12] C. Di Pisa and M. H. Aliabadi. An efficient BEM formulation for analysis of bond-line cracks in thin walled aircraft structures. *International Journal of Fracture*, 179(1-2):129–145, 2012. ISSN 0376-9429 1573-2673. doi: 10.1007/s10704-012-9782-3.

[13] S. Guimaraes and J. C. F. Telles. The method of fundamental solutions for fracture mechanics—reissner's plate application. *Engineering Analysis with Boundary Elements*, 33(10):1152–1160, 2009. ISSN 09557997. doi: 10.1016/j.enganabound.2009.04.010.

[14] X. Peng, E. Atroshchenko, P. Kerfriden, and S. P. A. Bordas. Linear elastic fracture simulation directly from CAD: 2D NURBS-based implementation and role of tip enrichment. *International Journal of Fracture*, 204(1):55–78, 2016. ISSN 0376-9429 1573-2673. doi: 10.1007/s10704-016-0153-3.

[15] V. Mallardo, E. Ruocco, and G. Beer. A NURBS-BEM application in continuum damage mechanics. In *Key Engineering Materials*, volume 774, pages 253–258, 2017.

[16] K. V. Kostas, A. I. Ginnis, C. G. Politis, and P. D. Kaklis. Shape-optimization of 2D hydrofoils using an isogeometric BEM solver. *Computer-Aided Design*, 82:79–87, 2017. ISSN 00104485. doi: 10.1016/j.cad.2016.07.002.

[17] S. Rahman and G. Chen. Continuum shape sensitivity and reliability analyses of nonlinear cracked structures. *International Journal of Fracture*, 131(2):189–209, 2005. ISSN 0376-9429 1573-2673. doi: 10.1007/s10704-004-3948-6.

[18] B. N. Rao and S. Rahman. Continuum shape sensitivity analysis of a mixed-mode fracture in functionally graded materials. *Computer Methods in Applied Mechanics and Engineering*, 194(18-20):1913–1946, 2005. ISSN 00457825. doi: 10.1016/j.cma.2004.06.027.

[19] R. M. Reddy and B. N. Rao. Stochastic fracture mechanics by fractal finite element method. *Computer Methods in Applied Mechanics and Engineering*, 198(3-4):459–474, 2008. ISSN 00457825. doi: 10.1016/j.cma.2008.08.014.

[20] M. S. Chowdhury, C. Song, and W. Gao. Probabilistic fracture mechanics with uncertainty in crack size and orientation using the scaled boundary finite element method. *Computers and Structures*, 137:93–103, 2014. ISSN 00457949. doi: 10.1016/j.compstruc.2013.03.002.

[21] M. S. Chowdhury, C. Song, W. Gao, and C. Wang. Reliability analysis of homogeneous and bimaterial cracked structures by the scaled boundary finite element method and a hybrid random-interval model. *Structural Safety*, 59:53–66, 2016. ISSN 01674730. doi: 10.1016/j.strusafe.2015.11.003.

[22] M. S. Edke and K. Chang. Shape sensitivity analysis for 2D mixed mode fractures using Extended FEM (XFEM) and Level Set Method (LSM). *Mechanics Based Design of Structures and Machines*, 38(3):328–347, 2010. ISSN 1539-7734 1539-7742. doi: 10.1080/15397731003744579.

[23] S. Rahman and B. N. Rao. Probabilistic fracture mechanics by Galerkin meshless methods - part II: reliability analysis. *Computational Mechanics*, 28(5):365–374, 2002. ISSN 0178-7675 1432-0924. doi: 10.1007/s00466-002-0300-8.

[24] B. N. Rao and S. Rahman. Probabilistic fracture mechanics by Galerkin meshless methods - part I: rates of stress intensity factors. *Computational Mechanics*, 28(5):351–364, 2002. ISSN 0178-7675 1432-0924. doi: 10.1007/s00466-002-0299-x.

[25] X. Huang and M. H. Aliabadi. Probabilistic fracture mechanics by the boundary element method. *International Journal of Fracture*, 171(1):51–64, 2011. ISSN 0376-9429 1573-2673. doi: 10.1007/s10704-011-9625-7.

[26] G. K. Sfantos and M. H. Aliabadi. A boundary element sensitivity formulation for contact problems using the implicit differentiation method. *Engineering Analysis with Boundary Elements*, 30(1):22–30, 2006. ISSN 09557997. doi: 10.1016/j.enganabound.2005.08.004.

[27] L. Morse, Z. Sharif Khodaei, and M. H. Aliabadi. A multi-fidelity boundary element method for structural reliability analysis with higher-order sensitivities. *Engineering Analysis with Boundary Elements*, 104: 183–196, 2019. ISSN 09557997. doi: 10.1016/j.enganabound.2019.03.036.

[28] J. C. F. Telles. A self adaptive coordinate transformation for efficient numerical evaluation of general boundary element integrals. *International Journal for Numerical Methods in Engineering*, 24(5):959–973, 1987. ISSN 00295981. doi: 10.1002/nme.1620240509.

[29] R. H. Rigby and M. H. Aliabadi. Decomposition of the mixed-mode J-integral - revisited. *International Journal of Solids and Structures*, 35(17):2073–2099, 1998. ISSN 00207683. doi: 10.1016/s0020-7683(97)00171-6.

[30] J. Iott, R. T. Haftka, and H. M. Adelman. Selecting step sizes in sensitivity analysis by finite difference. Report, National Aeronautics and Space Administration, 1985.

[31] R. Melchers. *Structural Reliability Analysis and Prediction*. John Wiley and Sons, 1999.

[32] T. Dirgantara and M. H. Aliabadi. Numerical simulation of fatigue crack growth in pressurized shells. *International Journal of Fatigue*, 24:725–738, 2002.